Structure of BRCA1-BRCT/Abraxas complex reveals phosphorylation-dependent BRCT dimerization at DNA damage sites

Qian Wu[1,6], Atanu Paul[2,3,6], Dan Su[2], Shahid Mehmood[4], Tzeh Keong Foo[5], Takashi Ochi[1], Emma L. Bunting[1], Bing Xia[5], Carol V. Robinson[4], Bin Wang[2,3,*], Tom L. Blundell[1*]

1 Department of Biochemistry, 80 Tennis Court Road, University of Cambridge, CB2 1GA, Cambridge, UK.
2 Departments of Genetics, The University of Texas MD Anderson Cancer Center, 1515 Holcombe Blvd, Houston, TX 77030
3 Genes and Development Program, The Graduate School of Biomedical Sciences at Houston, 6767 Bertner Ave, Houston, TX 77030
4 Department of Chemistry, Physical and Theoretical Chemistry Laboratory, University of Oxford, Oxford, UK.
5 Department of Radiation Oncology, Rutgers Cancer Institute of New Jersey and Robert Wood Johnson Medical School, 195 Little Albany Street, New Brunswick, NJ 08903.
6 Co-first authors

Corresponding authors: Tom Blundell: tom@cryst.bioc.cam.ac.uk; Bin Wang: bwang3@mdanderson.org

Summary

BRCA1 accumulation at DNA damage sites is an important step for its function in the DNA damage response and in DNA repair. BRCA1-BRCT domains bind to proteins containing the phosphorylated serine-proline-x-phenylalanine (pSPxF) motif including Abraxas, Bach1/FancJ and CtIP. In this study, we demonstrate that ionizing radiation (IR)-induces ATM-dependent phosphorylation of serine 404 (S404) next to the pSPxF motif. Crystal structures of BRCT/Abraxas show that phosphorylation of S404 is important for extensive interactions through the N-terminal sequence outside

the pSPxF motif and leads to formation of a stable dimer. Mutation of S404 leads to deficiency in BRCA1 accumulation at DNA damage sites and cellular sensitivity to IR. In addition, two germline mutations of BRCA1 are found to disrupt the dimer interface and dimer formation. Thus, we demonstrate a mechanism involving IR-induced phosphorylation and dimerization of the BRCT/Abraxas complex for regulating Abraxas-mediated recruitment of BRCA1 in response to IR.

Introduction

Patients with hereditary breast and ovarian cancer (HBOC) have high germline gene-mutation rates on chromosome 17q21 tumor suppressor gene *BRCA1* (breast cancer susceptibility genes 1) (Futreal et al., 1994; Hall et al., 1990; Miki et al., 1994). BRCA1 stabilizes genomic integrity by interacting with various DNA damage response (DDR) sensors, mediators and effector proteins, thereby coordinating recognition of the DNA damage sites, cell cycle checkpoint, DNA repair, transcription and apoptosis/senescence. BRCA1, a large protein of 1863 amino acids, contains an N-terminal RING domain and two C-terminal tandem BRCT domains. BRCT domains can recognize phosphorylated proteins with a pSPxF motif (Manke et al., 2003; Rodriguez et al., 2003; Yu et al., 2003) including Abraxas (Kim et al., 2007a; Liu et al., 2007; Wang et al., 2007), Bach1/FancJ (Cantor et al., 2001; Yu et al., 2003) and CtIP (Wong et al., 1998; Yu et al., 1998). The phosphopeptide-binding ability of BRCA1 BRCT is essential for BRCA1's tumor suppression function (Shakya et al., 2011), where many breast and ovarian cancer related mutations occur (Clapperton et al., 2004; Couch and Weber, 1996; Friedman et al., 1994; Shattuck-Eidens et al., 1995; Shiozaki et al., 2004; Williams et al., 2004).

The two BRCA1-BRCT domains (BRCT1 and BRCT2) each contain about 100 residues and associate in a head-to-tail manner (Williams et al., 2001). Structural analysis of BRCA1-BRCT domains with pSPxF-containing phosphopeptides of Bach1 (Clapperton et al., 2004, Shiozaki et al., 2004;), CtIP (Varma et al., 2005), syntheic optimized phosphopetide (Williams et al., 2004) or other binding proteins (Campbell et al., 2010; Liu and Ladias, 2013; Shen and Tong, 2008) have revealed that phosphorylated serine and phenylalanine in the pSPxF motif bind in a cleft formed at the junction of two BRCT domains in a "two-anchor" mode and the structural integrity of both binding sites is essential for peptide recognition (Glover et

al., 2004; Leung and Glover, 2011; Wu et al., 2015). However, little information exists regarding the importance of the sequence sourrounding the pSPxF motif. Nor is it known how the specificity is determined for BRCT binding to different pSPxF motif-containing proteins.

Abraxas mediates the interaction of BRCA1 to other components of the BRCA1-A complex, which include BRCC36, NBA1/MERIT40, BRE and Rap80. Abraxas, a 409-residue polypeptide, contains a non-catalytic MPN (Mpr1, Pad1 N-terminal) domain at its N-terminus, followed by a coiled-coil (CC) region, an unstructured region and a BRCA1-binding pSPTF motif at the C-terminus. While the N-terminal region including the MPN domain binds to Rap80, BRE and NBA1/MERIT40, the coil-coil domain is required for interaction with BRCC36 (Hu et al., 2011; Kim et al., 2007a; Wang and Elledge, 2007; Wang et al., 2009). Although the structures for BRCA1 BRCT in complex with other phosphopeptides have been solved previously (Campbell et al., 2010; Clapperton et al., 2004; Liu and Ladias, 2013; Shen and Tong, 2008; Shiozaki et al., 2004; Varma et al., 2005; Williams et al., 2004), the structure for BRCT/Abraxas has remained unknown.

Abraxas and the BRCA1-A complex recruits BRCA1 to DNA-damage double-stand-break sites (DSBs) in an ATM-dependent ubiquitin-mediated signaling pathway involving E2 conjugase Ubc13, E3 ligases RNF8/RNF168 and Rap80 binding to ubiquitin lys63-linked polyubiquitin conjugates (Doil et al., 2009; Harper and Elledge, 2007; Hu et al., 2012; Huen and Chen, 2007; Kim et al., 2007b; Kolas et al., 2007; Lee and Paull, 2004; Mailand et al., 2007; Sato et al., 2009; Uziel et al., 2003; Wang, 2012; Wang and Elledge, 2007; Wu et al., 2009). Abraxas-deficient mice exhibit decreased survival and increased tumor incidence (Castillo et al., 2014). The interaction of Abraxas with BRCA1 has been shown critical for the function of Abraxas in DNA repair of DSBs and maintenance of genomic stability. Mutation of the serine residue in the pSPxF motif leads to defective DNA repair and chromosome aberration. The importance of the Abraxas-BRCA1 interaction in tumor suppression is also suggested by identification of an Abraxas mutation in tumor in the phenylalanine residue of the pSPxF motif (F409C) (Castillo et al., 2014). Thus, structural and functional analysis of Abraxas and BRCA1 interaction is necessary to facilitate the understanding of Abraxas-mediated BRCA1 signaling in tumor suppression.

In this study, we have solved the crystal structures of BRCT with Abraxas

phosphorylated peptides and revealed an IR-induced, ATM-dependent Abraxas phosphorylation mechanism, which promotes dimerization of BRCT/Abraxas complex at the DNA damage sites. The IR-induced phosphorylation of Abraxas and the subsequent stabilization of BRCA1-BRCT dimerization are likely to comprise an important mechanism for accumulation of BRCA1 to DNA-damaged chromatin and BRCA1 mediated tumor suppression.

Results

Abraxas is double phosphorylated at S404 and S406 residues in response to IR

Analysis of the C-terminal sequence of Abraxas reveals an additional serine (S404) located close to the pSPxF motif (Figure 1A). Double-phosphorylated Abraxas peptide containing phosphorylated S406 and S404 (GFGEYpS^{404}RpS^{406}PTF) has been identified to bind to BRCA1-BRCT domains in response to IR (Wang et al., 2007). We decided to investigate whether the S404 residue is important and whether it is phosphorylated upon IR. Previously we have generated S406 phospho-specific antibody and showed that phosphorylation of S406 (pS406) occurs independently of IR (Wang et al., 2007). In view of the fact that S406 is nearby and is phosphorylated in the presence and absence of IR, we generated antibodies specifically recognizing double-phosphorylated S404 and S406 (pS404pS406). The pS404pS406 specific antibody recognized Abraxas in parental but not Abraxas knockout 293T cells and the intensity of the Abraxas band increased significantly when cells were treated with IR, indicative of IR-induced phosphorylation (Figure 1B). Mutation of either S404 (S404A), S406 (S406A) or double mutation (S404A, S406A) abolished the recognition of Abraxas by the pS404pS406 antibody (Figure 1C). Upon IR treatment, double phosphorylation of Abraxas S404 and S406 residues increased immediately (within 10 minutes), peaked at 1 h and gradually decreased to nearly basal levels at later time points (Figure 1D). Furthermore, double phosphorylation occurs in a dose-dependent manner in response to IR (Figure 1E). Since phosphorylation of S406 is not changed upon IR treatment, phosphorylation of S404 is likely to be IR-induced. As ATM plays a central role in the IR-induced signaling pathway that recruits Abraxas and the BRCA1-A complex (Harper and Elledge, 2007), we investigated whether ATM regulates the phosphorylation. Indeed, the IR-induced S404 phosphorylation is ATM dependent, treatment of an ATM inhibitor KU55933

completely abolished the IR-induced phosphorylation (Figure 1F). Other DNA damage response kinases including ATR, DNA-PK, Chk1 or Chk2, however, did not appear to have a major effect on the-IR induced phosphorylation recognized by the pS404pS406 antibody (Figure 1G and S1).

Crystal structures of BRCA1 BRCT domains in complex with single and double phosphorylated Abraxas peptides

Since S404 is separated by just one residue from S406, which is part of the pSPxF motif, we hypothesized that an additional mechanism exploiting phosphorylation of S404 might regulate Abraxas interaction with BRCA1. In order to test this we used structural information to allow comparison of the interactions between BRCT and Abraxas in single and double phosphorylated states. We solved crystal structures of BRCA1-BRCT in complex with both single (1p) and double-phosphorylated (2p) synthesized Abraxas peptides (Ab). The BRCT-Ab1p (GFGEYSRpSPTF) complex crystal was solved at 3.5 Å resolution with no clear main-chain electron density for the N-terminal GFGE region of the peptide, indicating that this region is flexible. BRCT-Ab1p_short without the GFGE residues (YSRpSPTF) complex was then crystalized and solved at 2.5 Å resolution. The structure of BRCT domains in complex with the double phosphorylated Abraxas peptide (Ab2p: GFGEYpSRpSPTF) was solved at 3.5 Å resolution. However, the BRCT-Ab2p_short (YpSRpSPTF) crystal did not diffract to a high resolution. We therefore used BRCT-Ab1p_short and BRCT-Ab2p structures (Figure 2A, S2A) for analysis. Statistics of these two structures are shown in Supplemental Table S1.

As in structures solved previously (Campbell et al., 2010; Clapperton et al., 2004; Liu and Ladias, 2013; Shen and Tong, 2008; Shiozaki et al., 2004; Varma et al., 2005; Williams et al., 2001, 2004), two BRCT domains of BRCA1 (BRCT1 and BRCT2) associate in a head-to-tail manner in both structures. In each domain, a four-stranded parallel β-sheet is surrounded by three α-helices with α1 and α3 on one side of the β-sheet and α2 on the other side. Helices α2 (from BRCT1), α′1 and α′3 (from BRCT2) form the hydrophobic interface, and the two domains are further linked by extra helix αL (Figure 2A, E). The pSPTF motif from Abraxas binds to the BRCT domains in a similar "two-anchor" mode using pS406 and F409. Residues P407 and T408 do not make major interactions with the BRCT domains. The phosphate group of Abraxas S406 interacts with the side chains of BRCT K1702 and S1655, as well as

the main chain of G1656 (Figure 2B). The side chain of F409 in Abraxas inserts into the BRCT hydrophobic pocket created by L1701, F1704, N1774, M1775 and L1839 (Figure 2C). As F409 is the terminal residue for Abraxas, an extra salt bridge is present between the main chain carboxyl group of F409 with the BRCT domain residue R1699 (Figure 2D). This extra interaction was seen in previous structures using tetrapeptides pSPTF (Campbell et al., 2010).

A notable difference between BRCT-Ab2p and BRCT-Ab1p_short structure is the conformation of the $Y^{403}S^{404}R^{405}$ region (Figure 2E, F and G). Extra electron density corresponding to the phosphate group of pS404 and the side chain of Y403 is observed only in BRCT-Ab2p. Unlike pS406, the pS404 phosphate group is oriented away from the BRCT domains into the solvent region, thus avoiding contact with G1656, L1657 and T1658 (Figure 2G). In BRCT-Ab2p, the Y403 side chain is positioned to interact through a hydrophobic interaction with BRCT P1659 at the N-terminus of BRCT1 α1. The extra interaction could explain the increased proximity of α1 towards the N-terminus of the Abraxas phosphopeptide in BRCT-Ab2p compared to BRCT-Ab1p_short (Figure S3A). Superimposition of all available BRCA1 BRCT related crystal structures also showed that α1 movement towards the phosphopeptide is most prominent in BRCT-Ab2p (Figure S2B). It indicates that one of the roles of pS404 is to fix the side chain of Y403, which is conserved in higher organisms (Figure 2I), such that a *trans* peptide bond can form and collision is avoided. Superimposition of the BRCT/Abraxas structures with the BRCT/Bach1 (PDB code:1T29) (Shiozaki et al., 2004) and BRCT/CtIP structures (PDB code: 1Y98) (Varma et al., 2005) shows similar pSPxF-motif binding. However, compared to Bach1 and CtIP, the N-terminal sequence of Abraxas in both BRCT-Ab1p and BRCT-Ab2p structures exits on the opposite side, close to the α1 of BRCT1 domain (Figure 2H). Interestingly, a similar side chain arrangement was also seen in BRCA1 BRCT bound with "optimized peptide" (GAAYDIpSQVFPFAKKK) (PDB code: 1T2V) (Williams et al., 2004) (Figure S3C), in which the tyrosine residue (Y) at -3 position (phosphorylated serine in pSxxF motif as 0 position) and negatively charged residues glutamic acid (E) or aspartic acid (D) at -2 position were shown more favored for interaction with BRCA1 BRCT domains (Manke et al., 2003; Rodriguez et al., 2003).

Dimerization of BRCT-Abraxas complex in crystal structures

There are eight copies of BRCT-Ab2p in the asymmetric unit (ASU), and each BRCT-Ab2p appears to dimerize through the same interface either within the ASU or between asymmetric units (Figure S2B). The dimerization of the 1:1 BRCT-Ab2p complex results in a 2:2 BRCT/Abraxas complex dimer. Dimerization involves α1 and β2 of the BRCT1 domain and the Ab2p (Figure 3A, B, C, D) burying about 1880 $Å^2$ area. In the dimer interface, two of the α1 helices from each BRCT-Ab2p complex form isologous interactions burying a hydrophobic patch formed by F1662, M1663 and Y1666 with aromatic side chains stacking on each other (Figure 3B). Interestingly, BRCA1 germline mutations of F1662 (F1662S) and M1663 (M1663K) have been identified in germline cancer patients as recorded in the Breast Cancer Information Core database (Szabo et al., 2000). Extensive hydrogen bonds also form between the two equivalent antiparallel β2 strands (Residues T^{1675}-L^{1679}) (Figure 3D). The two-fold symmetry axis within the BRCA1/Abraxas dimer lies perpendicular to the two β-strands. The cross interaction between the two BRCT/Abraxas complexes is also mediated by the ionic interaction between Abraxas and BRCT α1 of the opposite BRCT/Abraxas complex. The negative surface patch, generated by the phosphate group of pS404 and side chain of E402 at the N-terminus of Ab2p peptide, leads to cross interaction with BRCT K1671 (Figure 3C). The phosphate group of pS406 also contributes to the dimer formation by interacting with the R1670 residue of the opposite BRCT (Figure 3C). Although a similar dimer interface was observed for BRCT-Ab1p_short structure, the cross interaction between the negative surface patch (formed by the phosphate group of pS404 and the side chain of E402) and BRCT K1671 is completely lacking.

Compared to the monomeric BRCT/Abraxas complex, where pS406 is half surrounded by BRCT1 and half exposed to the solvent, the dimerization of BRCT/Abraxas allows the second BRCT1 to reduce further the accessibility of pS406 to solvent (Figure 3E).

BRCT/double-phosphorylated Abraxas complex forms a dimer *in vitro*

To examine whether the BRCT/Abraxas complex exists as a dimer *in vitro*, we first tested whether dimers form in solution using size exclusion chromatography at protein concentration (1 mg/ml), much lower than the concentration used for crystallization (30 mg/ml). The elution profiles of BRCT-Ab1p and BRCT-Ab2p were different. The BRCT-Ab2p elution peak appeared to the left of the BRCT-Ab1p

peak (Figure 3E), suggesting a larger hydrodynamic radius and a possible higher order BRCT-Ab2p complex. The controls show that BRCT does not interact with unphosphorylated Abraxas peptide or phosphopeptide containing only phosphorylated S404 (Figure S3A). Under the same condition, the BRCT-Bach1 and BRCT-CtIP form complexes similar to that of BRCT-Ab1p (Figure 3F). Standard protein markers were also run and the positions of their elution peaks are indicated in Figure 3F. The size of BRCT-Ab2p is roughly double that of BRCT-Ab1p according to the protein markers.

We tested whether a higher concentration of BRCT-Ab1p leads to dimer formation as we observed in crystals. Indeed, the BRCT-Ab1p peak shifts left to the BRCT-Ab2p peak position once the concentration is increased (Figure S3B), indicating the tendency of BRCT-Ab1p to form higher order complexes at high protein concentrations as observed in the crystal structure. It is likely that at high concentrations, the BRCT-Ab1p complex is packed in a conformation that is not stable at low protein concentrations without a contribution from phosphorylated S404. Therefore stable dimerization of two BRCT/Abraxas complexes is unique for BRCT-Ab2p.

To confirm dimer formation, we also measured the exact molecular weight of peak fractions eluted from gel filtration using nano-electrospray mass spectrometry analysis under native conditions (Figure 3G, H). BRCT-Ab1p is shown to exist predominantly as a 1:1 complex with a small portion forming a 2:2 dimer. In contrast, the majority of BRCT-Ab2p is detected as 2:2 complexes, indicating a much more stable dimer. BRCT/Bach1 and BRCT/CtIP are detected only as 1:1 complexes. Consistent with the finding that higher protein concentration facilitates dimer formation (Figure 4B), the proportion of BRCT-Ab1p forming dimer increases significantly when the protein concentration is increased from 15 μM to 75 μM (Figure S3F). Small angle X-ray scattering (SAXS) experiments of the BRCT-Ab1p and BRCT-Ab2p also show similar results (Figure S4). Thus, our results indicate that only double-phosphorylated Abraxas C-terminal peptide induces stable dimerization of BRCT/Abraxas complexes *in vitro*.

Mutagenesis studies of BRCT-Ab2p dimer interface reveal the importance of S404 phosphorylation and residues of BRCA1 germline mutations for stable BRCT/Abraxas dimer formation

In order to test the dimer interface, we have generated various mutants for both BRCT domains and Abraxas (summarized in Figure 4C with peptide sequence indicated) based on the crystal structure. As shown in a simplified graph of the dimer interface (Figure 4A), three regions of interactions appear to contribute to formation of the dimer interface: 1) the N-terminal hydrophobic region of BRCT α1-α1; 2) extensive hydrogen bonds formed by β2-β2; 3) the N-terminal region of Ab2p including the phosphorylated S404 interaction with BRCT α1. The interacting residues in α1-α1 and Ab2p-α1 are shown in Figure 4B.

By size exclusion chromatography, we first tested the importance of S404 phosphorylation. Mutations of Abraxas S404 to proline and aspartic acid were tested. While BRCT-Ab1p (S404P) leads to 1:1 complex formation, BRCT-Ab1p (S404D) can maintain the 2:2 complex dimer as BRCT-Ab2p (Figure 4D). This confirms that S404 phosphorylation is essential for dimerization. A previous report using optimized peptide containing aspartic acid in the equivalent position to Abraxas S404 was reported not forming dimer in solution (Williams et al., 2004). We reasoned that the difference between the optimized peptide and Ab2p is in the N-terminal region ($G^{399}F^{400}G^{401}E^{402}$) of Ab2p. We demonstrated that BRCT-Ab2p_short without GFGE still forms a dimer indicating that GEGE is not absolutely required for dimerization when Y^{403} and pS^{404} are present. However, when we analyzed BRCT-Ab2p in solution, we found that while F400D did not affect dimer formation, E402R as well as BRCT K1671E, R1670E partially destabilizes dimer formation and double mutation of BRCT(K1671E)-Ab2p(E402R) further destabilized the complex, eluting at a position close to that of 1:1 stoichiometry (Figure 4E). These results indicate that although GFGE is not absolutely required for the dimer formation, it contributes to the dimer stabilization when it is present.

We also tested the importance of the BRCT P1659 interaction with Abraxas Y403 to the stability of the BRCT-Ab2p dimer. In the presence of the N-terminal region (GFGE) of Ab2p, mutation of Abraxas Y403A did not destabilize the dimer complex formation in either BRCT-Ab2p(Y403A) or BRCT(P1659G)-Ab2p(Y403A). But when the N-terminal region of Abraxas was absent, the dimer complex of BRCT-Ab2p(Y403A_short) became unstable. This destabilization was further enhanced in BRCT(P1659G)-Abraxas(Y403A)_short complex, which was eluted near the 1:1 complex (Figure 4F). Together, these results are consistent with the crystal structure

analysis showing that double-phosphorylated Ab2p promotes dimer formation in two different ways: 1) phosphorylated S404 fixes the side chain of Y403, which generates additional interaction with BRCT K1671; 2) the phosphorylated group of pS404 and E402 form a negative surface region that leads to cross interaction with BRCT K1671.

We then evaluated the contribution of the hydrophobic interactions between the α-helices (α1-α1) and the extensive hydrogen bonds between the two antiparallel β strands (β2-β2) in the two protomers that comprise the dimer (Figure 4G). Our results indicate that the α1-α1 interaction contributes more significantly towards the stabilization of the dimer interface than the β2-β2 interaction. The BRCT mutant N1678A, which disrupted the β2-β2 interaction (Figure 3D), reduced hydrogen bonds between the side chain of N1678 and the nearby residue T1675, but did not destabilize BRCT-Ab2p dimer formation. In contrast, F1662S and M1663K, two BRCA1 germline mutations identified in cancer patients (Szabo et al., 2000), led to complete disruption of the dimer formation as the elution peaks of these two mutants in complex with Ab2p moved to the 1:1 complex position. BRCT Y1666A mutant did not result in complete disruption of the dimer and the peak in the elution profile is located between that for the 2:2 and 1:1 complexes. These results support our observation from the crystal structure that F1662S and M1663K have a much more significant effect on disruption of the dimer interface because these two residues are located at the point of the isologous dimer interface while Y1666A is further away.

Abraxas S404 is important for cellular resistance to IR and accumulation of BRCA1 at the DNA damage site

Since IR-induced phosphorylation of S404 appears to promote stable BRCT/Abraxas dimer formation, the S404 residue is likely to be critical for the function of Abraxas in response to IR. We first tested whether S404 is important for the cellular response to IR. In an IR sensitivity assay, both S404A and S406A mutants of Abraxas were unable to fully rescue the increased sensitivity of Abraxas knockdown cells as the wild-type Abraxas did (Figure 5A, 5B and S5), suggesting that phosphorylation of S404 plays a role in the cellular resistance to IR. Abraxas recruits BRCA1 to DNA damage sites in response to IR. We thus examined the role of S404 phosphorylation in BRCA1 accumulation at the DNA damage sites. The percentage of cells containing more than 10 BRCA1 IR-induced foci (IRIF) as well as the intensity of the foci were

significantly decreased in Abraxas knockdown cells. While the defect of Abraxas knockdown cells in BRCA1 IRIF formation could be rescued by expression of wild-type Abraxas, it could not be rescued by expression of Abraxas S406A or S404A mutant (Figure 5C, D and S5). Consistently, when we examined the chromatin-bound BRCA1 levels in response to IR, we found that the S404A mutant failed to accumulate BRCA1 to damaged chromatin in a similar way to the S406A mutant compared with the wild-type Abraxas does (Figure 5E). As a control, we demonstrated that the total expression level of BRCA1 was not affected in Abraxas knockdown cells or the cells complemented with expression of either wild type or mutants Abraxas. Thus, phosphorylation of S404 is likely to play an important role in BRCA1 accumulation to DNA damage sites and in cellular resistance to IR.

Abraxas-dependent BRCA1 dimerization *in vivo*

We tested whether BRCA1 forms dimers *in vivo* and whether the stable dimer formation is dependent on Abraxas. We co-expressed differentially Myc- or Flag-tagged BRCA1 full-length protein in control (Ctrl) cells or Abraxas knockout (KO) cells. In the co-immunoprecipitation experiment with lysates prepared from cells treated with IR, immunoprecipitated Flag-BRCA1 interacts with Myc-tagged BRCA1 indicating that BRCA1 indeed dimerizes *in vivo*. The dimerization was decreased in Abraxas knockout cells indicating the dependency of dimerization on Abraxas (Figure 6A). Similarly, a construct containing only the BRCA1-BRCT domains also dimerizes when co-expressed in cells and the dimerization is decreased in Abraxas knockout cells (Figure 6B).

We then tested whether the germline mutations F1662S and M1663K interfere with BRCA1 dimerization *in vivo*. We compared the interaction of a Myc-tagged full-length BRCA1 and a HA-tagged wild-type BRCT fragment with that of the F1662S or M1663K mutant of BRCA1 and a mutant BRCA1 BRCT fragment with three residues localized in the dimer interface mutated (F1662S/M1663K/R1670E). Both the Myc- immunoprecipitation (Figure 6C) and reciprocal HA- immunoprecipitation (Figure 6D) experiments showed that the interaction/dimerization of BRCA1 and BRCT was decreased with mutation of the critical residues at the dimer interface F1662S or M1663K. Thus, BRCA1 germline mutations interfere with stable dimer formation *in vivo*.

To understand dimerization of the BRCT/Abraxas complex *in vivo*, we examined whether Abraxas forms a dimer in which the phosphorylated C-termini of Abraxas in complex with BRCT could be in close vicinity for dimerization. We expressed both GFP-tagged Abraxas and HA-Flag-tagged Abraxas in cells and tested whether the differentially tagged Abraxas molecules interact with each other using the immunoprecipitation assay. We found that wild-type Abraxas, as well as the S404A and S406A mutant, interacts with differentially tagged counterpart, indicating that Abraxas dimerizes/oligomerizes *in vivo* independently of its binding to BRCA1 (Figure 6E). We then investigated what region of Abraxas mediates the dimerization by examining various deletion mutants of Abraxas. Deletion of the coiled-coil domain abolished the self-interaction of either wild-type or mutant Abraxas (Figure 6F and S6). Thus, *in vivo*, Abraxas dimerizes/oligomerizes through the coiled-coil domain.

Discussion

BRCA1 accumulation to DNA damage sites is a crucial step for BRCA1's function in DNA damage repair and BRCT domains of BRCA1 are important for the tumor suppressor function of BRCA1. IR-induced ubiquitination at DNA damages sites generates docking sites for the recruitment of the Abraxas/BRCA1-A complex and accumulation of BRCA1 at sites of damage. Our data provide evidence for an IR-induced, ATM-dependent mechanism specific to Abraxas-mediated recruitment of BRCA1. In such a model (Figure 7), IR-induced phosphorylation of S404 next to the pSPxF induces stable dimer formation of the BRCA1 BRCT/Abraxas complex.

The crystal structural analysis of BRCT in complex with Abraxas phosphorylated peptides revealed that, although both single phosphorylated Abraxas peptide Ab1p and double phosphorylated Ab2p bind to BRCT domains through the same pSPxF motif, the phosphorylation of S404 in Ab2p induces stable dimerization of the BRCT/Abraxas complex. The dimer interface locates to the BRCT1 of BRCA1 tandem BRCT domains. As expected from previous reports, BRCT1 also provides the interaction site for pS406 of the pSPxF motif while the side chain of F of the motif inserts into a hydrophobic pocket created mainly by BRCT2 domain. The dimer surface formed between two BRCT1 domains does not directly influence the interaction between the pSPxF motif and the BRCT domains. Although the hydrophobic α1 interface observed in the BRCT-Ab2p dimer was buried in a similar

manner in the BRCT-Ab1p or other BRCA1 BRCT related crystal structures to that previously described (Wu et al., 2015), this interaction is not strong enough to form a stable dimer in solution as we observed for BRCT domain only, BRCT-Ab1p, BRCT-Bach1 or BRCT-CtIP. In contrast, under the same condition, the stable-dimer state of BRCT-Ab2p is triggered by the phosphorylation of S404. A phosphorylation-mimetic point mutant S404D stabilizes BRCT/Abraxas dimer formation in solution in a similar way to phosphorylated S404, further supporting the conclusion that phosphorylation of S404 promotes dimer formation. The impact of phosphorylation of Abraxas S404 is the following: 1) the highly charged phosphate group of pS404 faces away from BRCT domains, resulting in stabilization of the interaction of the side chain of Y403 with BRCT P1659 located at the N-terminus of α1. This interaction causes the shift of α1 closer to the N-terminus of the phosphopeptide; 2) the negatively charged side chains of pS404 and E402 provide extra ionic interaction sites with K1671 of BRCT. All together, this leads to a stable BRCT-Ab2p complex dimer formation. Owing to the symmetric pairing shape, we describe the BRCT-Ab2p dimerization interaction as a "pair-hugging" interaction mode, in which the Abraxas phosphopeptide acts as an arm wrapping around the other BRCT domain therefore stabilizing the interaction (Figure 7).

The IR-induced phosphorylation of Abraxas S404 and the subsequent stable BRCA1-BRCT dimerization are likely to comprise an important mechanism for cellular response to IR since mutation of S404 leads to decreased BRCA1 accumulation to DNA damaged chromatin and increased cellular sensitivity to IR. IR−induced phosphorylation of Abraxas S404 may facilitate the accumulation of BRCA1 at DNA damage sites by stabilizing the BRCA1 protein dimerization forming more stable higher order complexes at sites of damage. In addition, S404 phosphorylation may further facilitate the interaction of Abraxas and BRCA1 by reducing the dissociation of pS406, so prolonging the Abraxas interaction with BRCT domains or limiting the accessibility of pS406 by other proteins such as phosphatase. Alternatively, induced dimerization of BRCA1 BRCT by phosphorylation of S404 of Abraxas could increase the local concentration of BRCA1 at damaged chromatin, which is likely critical for efficient DNA damage signaling and repair.

Many tumor-derived truncation and missense mutations have been identified in the BRCA1 BRCT domains. While some of these mutations have been shown to

either destabilize the protein fold of the BRCT domains or disrupt the binding surface to pSPxF-containing phosphopeptides (Cantor et al., 2001; Clapperton et al., 2004; Coquelle et al., 2011; Manke et al., 2003; Shiozaki et al., 2004; Williams and Glover, 2003; Williams et al., 2004; Yu et al., 2003), resulting in cancer predisposition, the function of a large number of BRCT mutations is still unknown (Easton et al., 2007). Our analyses reveal that germline mutations F1662S and M1663K disrupt the ability of BRCT to dimerize, *in vitro* and *in vivo*, providing a structural explanation for the possible role of these mutations in inactivating BRCA1 tumor suppressor function. Future study is needed to further characterize the effect of these mutations in the function of BRCA1 in DNA repair and damage signaling.

How is the dimerization of BRCT-Abraxas achieved *in vivo*? Since the phosphorylation of S406 is not IR-dependent, Abraxas binds to BRCA1 through the pSPxF motif even in the absence of DNA damage (Wang et al., 2007). The dimerization of Abraxas through the coiled-coil domain could potentially position the two BRCT tandem domains that interact at the C-terminus of Abraxas into close vicinity, leading to an unstable dimer of the BRCT-Abraxas complex in the absence of DNA damage. In response to IR, IR-induced phosphorylation of S404 leads to an increase of affinity between the phosphate group and the residues at the dimer surface, which consequently results in a much more stable dimer complex of BRCA1 BRCT/Abraxas. Since the coiled-coil domain of Abraxas also appears to dimerize with the coiled-coil domain of BRCC36 (Wang and Elledge, 2007), it is likely that, in the BRCA1-A complex, Abraxas and BRCC36 form an oligomeric bundle through the coiled-coil domain present on each of the Abraxas and BRCC36 molecule. Future structural analysis of the BRCA1-A complex is needed to further understand the multimerization of Abraxas and BRCC36 of the BRCA1-A complex. Nevertheless, IR-induced phosphorylation at Abraxas S404 appears to function as a regulatory switch, which leads to stable dimerization of two nearby BRCT domains.

The phosphorylation-induced BRCT dimerization is observed only in the BRCT/Abraxas complex. We demonstrate that, in addition to the pSPxF-binding motif, IR-induced phosphorylation of a nearby S404 residue can further regulate the interaction of BRCT and Abraxas. Thus, amino acid sequences outside the pSPxF motif may confer specificity in regulation of the BRCT binding to phosphorylated proteins. Indeed, in addition to phosphorylated S404, the N-terminal region of Abraxas peptide (GFGE^{402}Y^{403}pS^{404}RpSPVF) also contributes to stable

BRCT/Abraxas dimer formation. The E402 residue cooperates with the phosphorylated S404 in stabilizing the dimer formation; the side chain of Y403 is fixed to interact with BRCT P1659 when S404 is phosphorylated. Thus the unique sequence feature outside of the pSPxF motif ensures that stable dimer formation occurs only with BRCT/Abraxas but not with other BRCT complexes. Since Abraxas-BRCA1 interaction has been shown critical for DNA repair and maintenance of genomic stability, the additional regulatory mechanism uncovered in this study in regulating the interaction of Abraxas and BRCA1 further highlights the importance of this interaction in BRCA1 signaling and tumor suppression.

In summary, our study reveals a phosphorylation-dependent mechanism in Abraxas-mediated recruitment and accumulation of BRCA1 at DNA damage sites, deepening our understanding of BRCA1 and Abraxas tumor suppressor function and related cellular signaling. Our study also provides structural insights that will assist the design of small molecules modulating BRCA1-Abraxas interaction in the future.

Experimental Procedures

Cell Lines, Culture and Antibodies

U2OS cells were cultured in McCoy's 5A medium supplemented with 10% FBS. 293T cells were grown in Dulbecco's modified Eagles medium (DMEM) supplemented with 10% FBS. Details of generation of Abraxas knockdown or knockout cells were described in the supplemental methods. Antibodies used are described in the supplemental methods.

Immunofluorescence

Cells were fixed with 3.6% formaldehyde for 10 min, permeabilized with 0.5% Triton X-100 solution and incubated with primary antibodies for 1 hr at 37^{o}C followed by appropriate Alexa 488-conjugated (green; Invitrogen) and Alexa 555-conjugated (red; Invitrogen) secondary antibodies. Additional information is included in the supplemental methods.

Cell Lysis and Immunoprecipitation

Cell lysates were prepared from 293T cells or 293T Abra1-gene knockout cells either untreated or treated with 10 Gy IR followed by incubation at 37°C for 1 hr. Flag

immunoprecipitation (IP) was performed with lysates prepared from cells either treated or untreated with 10 Gy IR followed by 1 hr incubation at 37°C. Western blots were carried out using indicated antibodies. 293T cells were incubated with kinase inhibitors for 2 hr at indicated concentrations. Cells were then either exposed to 4 Gy IR or untreated. After 1 hr incubation, cells were lysed and Abraxas pS404pS406 levels were determined by western blot. Additional information is included in the supplemental methods.

Clonogenic Survival Assay

Stable U2OS cell lines were seeded at low density in 10 cm dishes and irradiated with 4 Gy ionizing irradiation using a ^{137}Cs source. The cells were then cultured at 37°C for 14 days to allow colonies to form. Colonies were stained with 2% methylene blue and 50% ethanol for 10 min.

Chromatin fractionation

Abraxas knockdown cells complemented with vector, WT, S404A, S406A and double mutant (S404A, S406A) were irradiated at 10 Gy and incubated for 1 hr at 37°C. Cells were then subjected for chromatin fractionation followed by detection with indicated antibodies. Details are described in the supplemental methods.

BRCT construct, purification, crystallization, and data collection

Construction and purification of BRCA1 BRCT and mutants are described in the supplemental data. Purified BRCT was mixed with Abraxas peptides at a 1:3 molar ratio as has been previously reported (Shiozaki et al., 2004) and incubated at 4ºC for 30 minutes. Final protein concentration was 30 mg/ml. Crystallization was set up using the hanging-drop vapour diffusion method with drops containing 1 µl of protein sample and 1µl of crystallization solution. Crystals appeared after 3-4 days. BRCT-Ab2p was crystallized in 0.1 M HEPES pH 7.0, 60 mM ammonium sulphate and 5% (w/v) PEG 4000. BRCT-Ab1p_short was crystallized in 1 M lithium chloride, 0.1 Tris pH 8.0 and 20% (w/v) PEG 6000. X-ray diffraction data were processed by *XDS* (Kabsch, 2010) and *scala* (Winn et al., 2011). The phases for the structure factors were obtained through molecular replacement using Phaser module in *Phenix 1.8.4-1496* (Adams et al., 2010). More detail of protein crystal and structure determination can be found in supplemental data.

Size exclusion chromatography for BRCT with Abraxas, Bach1 and CtIP phosphopeptides

BRCT protein and Abraxas, Bach1 and CtIP peptides were mixed in a 1:3 molar ratio to a final concentration of 1mg/ml (about 40 μM) in 500 μl loops. Gel filtration was performed in Buffer A using Superdex75 10/300 column (GE Healthcare life) with a flow rate of 0.5 ml/min. For studying the high protein concentration effects on BRCT-Abraxas complex formation, a final concentration of 10 mg/ml was used. Protein markers (GE Gel Filtration LMW Calibration Kit) were run following the kit protocol.

Native mass spectrometry

Samples were diluted to 15 or 75 μM protein concentration in 300 mM ammonium acetate pH 7.6 and further buffer exchanged into 300 mM ammonium acetate using Bio-Spin 6 (Bio-Rad) column. The desalted samples were loaded into the in-house prepared gold-coated glass capillaries (Hernández and Robinson, 2007). Nano-electrospray mass spectrometric analyses were performed under native conditions on a hybrid quadrupole time-of-flight mass spectrometer previously modified for high mass transmission (Sobott et al., 2002). Typically the following instrumental conditions were used: capillary voltage 1.3 kV, sample cone 200 V and collision cell energy 5 V.

Author Contributions

Q.W., B.W. and T.L.B. initiated this project. Q.W. performed most of the *in vitro* work and solved structures. A.P., D.S. and B.W. designed the *in vivo* experiments. D.S. generated Abraxas knockout cell and analyzed Abraxas double phosphorylation in response to IR and in the presence of kinase inhibitors, as well as Abraxas dimerization *in vivo*. A.P. generated Abraxas knockdown cells, examined the Abraxas mutants in rescuing the defects of Abraxas-deficient cells, and Abraxas-dependent BRCA1 dimerization *in vivo*. S.M. and C.V.R. performed and analyzed the native mass spectrometry experiment. T.O. conducted SAXS experiment. E.L.B. made and purified the BRCT P1659G mutant. T.K.F and B.X. generated constructs expressing Myc-tagged BRCA1 F1662S and M1663K mutants. Q.W., A.P., B.W., and T.L.B. wrote the paper together with comments from other coauthors.

Acknowledgments

We thank beamline scientists at Diamond Light Source for help during data collection of crystal and SAXS. The crystallization experiments were performed in the Crystallographic X-ray facility at the Department of Biochemistry, University of Cambridge. We are grateful to the Facility Manager, Dr. Dimitri Chirgadze, for his assistance in using these facilities and advice during crystal structure determination. We also thank Dr. Yanfen Hu (University of Texas Health Science Center at San Antonia) for the pFlag-BRCA1 plasmid and Dr. Angela Pacitto (University of Cambridge) for reading the manuscript. We thank Dr. Adriana Paulucci-Holthanuzen (Department of Genetics-MD Anderson Microscopy Core Facility) for assistance with images and analysis. Q.W., T.O. and T.L.B. are funded by the Wellcome Trust (Grant 093167/Z/10/Z). A.P. is an awardee of the Schissler Foundation Fellowship, the Center for Cancer Epigenetics Scholarship and the Andrew Sowell-Wade Huggins Scholarship. This work is supported by the National Institutes of Health grant (CA155025 to B.W) with funds from the University of Texas MD Anderson Cancer Center (IRG, Center for Cancer Epigenetics, Center for Genetics and Genomics Pilot Award). S.M. is funded by the Medical Research Council (grant 98101 to C.V.R.) and C.V.R. is a Royal Society Research Professor. T.K.F and B.X. are supported by National Institutes of Health grant (R01CA138804 to B.X).

The crystallographic models have been deposited in the Protein Data Bank under accession numbers 4Y18 ad 4Y2G.

References

Adams, P.D., Afonine, P. V., Bunkóczi, G., Chen, V.B., Davis, I.W., Echols, N., Headd, J.J., Hung, L.W., Kapral, G.J., Grosse-Kunstleve, R.W.G., et al. (2010). PHENIX: a comprehensive Python-based system for macromolecular structure solution. Acta Crystallogr. Sect. D *66*, 213–221.

Campbell, S.J., Edwards, R.A., and Glover, J.N.M. (2010). Comparison of the structures and peptide binding specificities of the BRCT domains of MDC1 and BRCA1. Structure *18*, 167–176.

Cantor, S.B., Bell, D.W., Ganesan, S., Kass, E.M., Drapkin, R., Grossman, S., Wahrer, D.C.R., Sgroi, D.C., Lane, W.S., Haber, D.A., et al. (2001). BACH1, a novel helicase-like protein, interacts directly with BRCA1 and contributes to its DNA repair function. Cell *105*, 149–160.

Castillo, A., Paul, A., Sun, B., Huang, T.H., Wang, Y., Yazinski, S.A., Tyler, J., Li, L., You, M.J., Zou, L., et al. (2014). The BRCA1-Interacting Protein Abraxas Is Required for Genomic Stability and Tumor Suppression. Cell Rep. *8*, 807–817.

603 Clapperton, J.A., Manke, I.A., Lowery, D.M., Ho, T., Haire, L.F., Yaffe, M.B., and Smerdon, S.J.
604 (2004). Structure and mechanism of BRCA1 BRCT domain recognition of phosphorylated BACH1
605 with implications for cancer. Nat. Struct. Mol. Biol. *11*, 512–518.

606 Coquelle, N., Green, R., and Glover, J.N.M. (2011). Impact of BRCA1 BRCT domain missense
607 substitutions on phosphopeptide recognition. Biochemistry *50*, 4579–4589.

608 Couch, F.J., and Weber, B.L. (1996). Mutations and polymorphisms in the familial early-onset breast
609 cancer (BRCA1) gene. Breast Cancer Information Core. Hum. Mutat. *8*, 8–18.

610 Doil, C., Mailand, N., Bekker-Jensen, S., Menard, P., Larsen, D.H., Pepperkok, R., Ellenberg, J.,
611 Panier, S., Durocher, D., Bartek, J., et al. (2009). RNF168 Binds and Amplifies Ubiquitin Conjugates
612 on Damaged Chromosomes to Allow Accumulation of Repair Proteins. Cell *136*, 435–446.

613 Easton, D., Deffenbaugh, A., Pruss, D., Frye, C., Wenstrup, R., Allen-Brady, K., Tavtigian, S.,
614 Monteiro, A., Iversen, E., Couch, F., et al. (2007). A systematic genetic assessment of 1,433 sequence
615 variants of unknown clinical significance in the BRCA1 and BRCA2 breast cancer-predisposition
616 genes. Am. J. Hum. Genet. *81*, 873–883.

617 Emsley, P., Lohkamp, B., Scott, W.G., and Cowtan, K. (2010). Features and development of Coot.
618 Acta Crystallogr. D. Biol. Crystallogr. *66*, 486–501.

619 Friedman, L.S., Ostermeyer, E.A., Szabo, C.I., Dowd, P., Lynch, E.D., Rowell, S.E., and King, M.-C.
620 (1994). Confirmation of BRCA1 by analysis of germline mutations linked to breast and ovarian cancer
621 in ten families. Nat. Genet. *8*, 399–404.

622 Fu, Y., Sander, J.D., Reyon, D., Cascio, V.M., and Joung, J.K. (2014). Improving CRISPR-Cas
623 nuclease specificity using truncated guide RNAs. Nat Biotech *32*, 279–284.

624 Futreal, P.A., Liu, Q., Shattuck-Eidens, D., Cochran, C., Harshman, K., Tavtigian, S., Bennett, L.M.,
625 Haugen-Strano, A., Swensen, J., and Miki, Y. (1994). BRCA1 mutations in primary breast and ovarian
626 carcinomas. Science *266*, 120–122.

627 Glover, J.N.M., Williams, R.S., and Lee, M.S. (2004). Interactions between BRCT repeats and
628 phosphoproteins: tangled up in two. Trends Biochem. Sci. *29*, 579–585.

629 Hall, J.M., Lee, M.K., Newman, B., Morrow, J.E., Anderson, L.A., Huey, B., and King, M.-C. (1990).
630 Linkage of early-onset familial breast cancer to chromosome 17q21. Science *250*, 1684–1689.

631 Harper, J.W., and Elledge, S.J. (2007). The DNA Damage Response: Ten Years After. Mol Cell *28*,
632 739–745.

633 Hernández, H., and Robinson, C. V. (2007). Determining the stoichiometry and interactions of
634 macromolecular assemblies from mass spectrometry. Nat. Protoc. *2*, 715–726.

635 Hu, X., Kim, J., Castillo, A., Huang, M., Liu, J., and Wang, B. (2011). NBA1/MERIT40 and BRE
636 Interaction Is Required for the Integrity of Two Distinct Deubiquitinating Enzyme BRCC36-containing
637 Complexes. J. Biol. Chem. *286*, 11734–11745.

638 Hu, X., Paul, A., and Wang, B. (2012). RAP80 recruitment to DNA double strand breaks requires
639 binding to both sumo- and ubiquitin-conjugates . J. Biol. Chem. *287*, 25510–25519.

640 Huen, M.S.Y., and Chen, J. (2007). The DNA damage response pathways: at the crossroad of protein
641 modifications. Cell Res. *18*, 8–16.

642 Kabsch, W. (2010). XDS. Acta Crystallogr. Sect. D *66*, 125–132.

643 Kim, H., Huang, J., and Chen, J. (2007a). CCDC98 is a BRCA1-BRCT domain-binding protein
644 involved in the DNA damage response. Nat. Struct. Mol. Biol. *14*, 710–715.

645 Kim, H., Chen, J., and Yu, X. (2007b). Ubiquitin-Binding Protein RAP80 Mediates BRCA1-
646 Dependent DNA Damage Response. Science (80-.). *316*, 1202–1205.

647 Kolas, N.K., Chapman, J.R., Nakada, S., Ylanko, J., Chahwan, R., Sweeney, F.D., Panier, S., Mendez,
648 M., Wildenhain, J., Thomson, T.M., et al. (2007). Orchestration of the DNA-Damage Response by the
649 RNF8 Ubiquitin Ligase. Science (80-.). *318*, 1637–1640.

650 Krissinel, E., and Henrick, K. (2007). Inference of macromolecular assemblies from crystalline state. J.
651 Mol. Biol. *372*, 774–797.

652 Lee, J.-H.H., and Paull, T.T. (2004). Direct activation of the ATM protein kinase by the
653 Mre11/Rad50/Nbs1 complex. Science *304*, 93–96.

654 Leung, C.C.Y., and Glover, J.N.M. (2011). BRCT domains: easy as one, two, three. Cell Cycle *10*,
655 2461–2470.

656 Liu, X., and Ladias, J.A.A. (2013). Structural basis for the BRCA1 BRCT interaction with the proteins
657 ATRIP and BAAT1. Biochemistry *52*, 7618–7627.

658 Liu, Z., Wu, J., and Yu, X. (2007). CCDC98 targets BRCA1 to DNA damage sites. Nat. Struct. Mol.
659 Biol. *14*, 716–720.

660 Mailand, N., Bekker-Jensen, S., Faustrup, H., Melander, F., Bartek, J., Lukas, C., and Lukas, J. (2007).
661 RNF8 Ubiquitylates Histones at DNA Double-Strand Breaks and Promotes Assembly of Repair
662 Proteins. Cell *131*, 887–900.

663 Manke, I.A., Lowery, D.M., Nguyen, A., and Yaffe, M.B. (2003). BRCT repeats as phosphopeptide-
664 binding modules involved in protein targeting. Science (80-.). *302*, 636–639.

665 Miki, Y., Swensen, J., Shattuck-Eidens, D., Futreal, P.A., Harshman, K., Tavtigian, S., Liu, Q.,
666 Cochran, C., Bennett, L.M., Ding, W., et al. (1994). A strong candidate for the breast and ovarian
667 cancer susceptibility gene BRCA1. Science *266*, 66–71.

668 Ran, F.A., Hsu, P.D., Wright, J., Agarwala, V., Scott, D.A., and Zhang, F. (2013). Genome engineering
669 using the CRISPR-Cas9 system. Nat. Protoc. *8*, 2281–2308.

670 Rodriguez, M., Yu, X., Chen, J., and Songyang, Z. (2003). Phosphopeptide Binding Specificities of
671 BRCA1 COOH-terminal (BRCT) Domains. J. Biol. Chem. *278*, 52914–52918.

672 Sato, Y., Yoshikawa, A., Mimura, H., Yamashita, M., Yamagata, A., and Fukai, S. (2009). Structural
673 basis for specific recognition of Lys 63-linked polyubiquitin chains by tandem UIMs of RAP80.
674 EMBO J. *28*, 2461–2468.

675 Shakya, R., Reid, L.J., Reczek, C.R., Cole, F., Egli, D., Lin, C.-S., DeRooij, D.G., Hirsch, S., Ravi, K.,
676 Hicks, J.B., et al. (2011). BRCA1 tumor suppression depends on BRCT phosphoprotein binding, but
677 not its E3 ligase activity. Science (80-.). *334*, 525–528.

678 Shattuck-Eidens, D., McClure, M., Simard, J., Labrie, F., Narod, S., Couch, F., Hoskins, K., Weber, B.,
679 Castilla, L., Erdos, M., et al. (1995). A collaborative survey of 80 mutations in the BRCA1 breast and
680 ovarian cancer susceptibility gene. Implications for presymptomatic testing and screening. JAMA *273*,
681 535–541.

682 Shen, Y., and Tong, L. (2008). Structural evidence for direct interactions between the BRCT domains
683 of human BRCA1 and a phospho-peptide from human ACC1. Biochemistry *47*, 5767–5773.

Shiozaki, E.N., Gu, L., Yan, N., and Shi, Y. (2004). Structure of the BRCT repeats of BRCA1 bound to a BACH1 phosphopeptide: implications for signaling. Mol. Cell *14*, 405–412.

Sobott, F., Hernández, H., McCammon, M.G., Tito, M.A., and Robinson, C. V. (2002). A Tandem Mass Spectrometer for Improved Transmission and Analysis of Large Macromolecular Assemblies. Anal. Chem. *74*, 1402–1407.

Szabo, C., Masiello, A., Ryan, J.F., and Brody, L.C. (2000). The Breast Cancer Information Core: Database design, structure, and scope. Hum. Mutat. *16*, 123–131.

Uziel, T., Lerenthal, Y., Moyal, L., Andegeko, Y., Mittelman, L., and Shiloh, Y. (2003). Requirement of the MRN complex for ATM activation by DNA damage. EMBO J. *22*, 5612–5621.

Varma, A.K., Brown, R.S., Birrane, G., and Ladias, J.A.A. (2005). Structural Basis for Cell Cycle Checkpoint Control by the BRCA1−CtIP Complex. Biochemistry *44*, 10941–10946.

Wang, B. (2012). BRCA1 tumor suppressor network: focusing on its tail. Cell Biosci. *2*.

Wang, B., and Elledge, S.J. (2007). Ubc13/Rnf8 ubiquitin ligases control foci formation of the Rap80/Abraxas/Brca1/Brcc36 complex in response to DNA damage. Proc. Natl. Acad. Sci. U. S. A. *104*, 20759–20763.

Wang, B., Matsuoka, S., Ballif, B.A., Zhang, D., Smogorzewska, A., Gygi, S.P., and Elledge, S.J. (2007). Abraxas and RAP80 Form a BRCA1 Protein Complex Required for the DNA Damage Response. Science (80-.). *316*, 1194–1198.

Wang, B., Hurov, K., Hofmann, K., and Elledge, S.J. (2009). NBA1, a new player in the Brca1 A complex, is required for DNA damage resistance and checkpoint control. Genes Dev. *23*, 729–739.

Williams, R.S., and Glover, J.N.M. (2003). Structural consequences of a cancer-causing BRCA1-BRCT missense mutation. J. Biol. Chem. *278*, 2630–2635.

Williams, R.S., Green, R., and Glover, J.N.M. (2001). Crystal structure of the BRCT repeat region from the breast cancer-associated protein BRCA1. Nat. Struct. Biol. *8*, 838–842.

Williams, R.S., Lee, M.S., Hau, D.D., and Glover, J.N.M. (2004). Structural basis of phosphopeptide recognition by the BRCT domain of BRCA1. Nat Struct Mol Biol *11*, 519–525.

Winn, M.D., Ballard, C.C., Cowtan, K.D., Dodson, E.J., Emsley, P., Evans, P.R., Keegan, R.M., Krissinel, E.B., Leslie, A.G.W., McCoy, A., et al. (2011). Overview of the CCP4 suite and current developments. Acta Crystallogr. Sect. D *67*, 235–242.

Wong, A.K., Ormonde, P.A., Pero, R., Chen, Y., Lian, L., Salada, G., Berry, S., Lawrence, Q., Dayananth, P., Ha, P., et al. (1998). Characterization of a carboxy-terminal BRCA1 interacting protein. Oncogene *17*, 2279–2285.

Wu, J., Huen, M.S., Lu, L.-Y.Y., Ye, L., Dou, Y., Ljungman, M., Chen, J., and Yu, X. (2009). Histone ubiquitination associates with BRCA1-dependent DNA damage response. Mol. Cell. Biol. *29*, 849–860.

Wu, Q., Jubb, H., and Blundell, T. (2015). Phosphopeptide interactions with BRCA1 BRCT domains: More than just a motif. Prog. Biophys. Mol. Biol. *117*, 143–148.

Yu, X., Wu, L.C., Bowcock, A.M., Aronheim, A., and Baer, R. (1998). The C-terminal (BRCT) domains of BRCA1 interact in vivo with CtIP, a protein implicated in the CtBP pathway of transcriptional repression. J. Biol. Chem. *273*, 25388–25392.

Yu, X., Chini, C.C.S., He, M., Mer, G., and Chen, J. (2003). The BRCT domain is a phospho-protein binding domain. Science *302*, 639–642.

Figure Legends

Figure 1: IR induced double phosphorylation of Abraxas C-terminus S404 and S406 is ATM-dependent. A) Abraxas-domain boundary and C-terminal sequence containing a serine residue (S404) next to the BRCA1-binding pSPxF motif (high-lighted in blue). CC represents coiled-coil domain. Phosphorylation of S404 and S406 is indicated as P. B) Double phosphorylation of S404 and S406 residues at the Abraxas C-terminus in response to IR in 293T cells and 293T/Abraxas knockout (KO) cells. Lysates from cells treated with 10 Gy IR followed by incubation at 37 °C for 1 h were used for western blot with anti-pS404pS406 antibody. "*" non-specific band. C) IR-induced double phosphorylation of S404 and S406 is abolished in Abraxas mutants (S404A, S406A or double mutant (DM)). "*" non-specific band. Flag- and HA-tagged Abraxas wild type (WT) or mutants were expressed in 293T cells. Lysates from cells treated with 10 Gy IR, incubated at 37 °C for 1 hr were used for immunoprecipitation with anti-Flag beads and western blot with antibodies against pS404pS406 and pS406 of HA. D) IR-induced double phosphorylation of S404 and S406 occurs immediately after IR treatment. Time-points were taken after cells were treated with 4 Gy IR followed by incubation at 37 °C. E) IR-induced phosphorylation occurs in a dose-dependent manner. F) ATM regulates IR-induced phosphorylation. Cells were incubated with ATM kinase inhibitor KU55933 (10 μM) for 2 hr before exposure to 4 Gy IR and subsequent incubation at 37°C for 1 hr. G) ATR is not involved in IR-induced double phosphorylation. ATR inhibitor VE-821 at indicated concentrations were used for treating cells for 2 hr before cells were exposed to 4 Gy IR. (See also Figure S1)

Figure 2: Crystal structures of BRCT in complex with single and double phosphorylated Abraxas peptides. A) Crystal structure of BRCT-Ab1p_short. BRCT domains are in yellow, and Ab1p_short peptide is in wheat. B) C) and D) show the detailed interactions between phosphopeptide and BRCT domains. Polar interaction is indicated in dashed lines. E) Crystal structure of BRCT-Ab2p. BRCT is in blue and Ab2p peptide is in cyan. F) and G) show the interface between BRCT and Abraxas peptide in both BRCT-Ab1p_short and BRCT-Ab2p structures. 2Fo-Fc electron density (σ=1.0) is shown for Abraxas peptides. H) Superimposition of

BRCT-Ab2p, BRCT-Ab1p_short, BRCT-Bach1 (PDB code: 1T29) and BRCT-CtIP (PDB code: 1Y98). BRCT domains are shown in a grey surface representation. Ab2p is in blue, Ab1p_short is in yellow, Bach1 is in green and CtIP is in purple. The pSPxF Motif is indicated. I) Sequence alignment of Abraxas C-terminus. BRCT-binding motif is indicated by a blue line. A black arrow indicates the half conserved residues. (See also Figure S2 and S3)

Figure 3: Double phosphorylated Abraxas peptide induces dimerization of BRCT-Ab2p complex. A) Crystal structure of BRCT-Ab2p complex dimer viewed from three different directions. The two-fold axis is shown as a black arrow. The dimer interface is within the dashed circles and zoomed in B, C and D. B) Dimer interface between two BRCT α1 helices. C) Interaction between BRCT α1 helix and Ab2p. D) Dimer interface between two BRCT β2 strands. Polar interactions between labelled residues are shown in black dashed line. Key residues are indicated. E) Surface representation of BRCA1-1p_short (yellow) and BRCT-Ab2p dimer (blue and pink). Abraxas pS406 binding region is indicated in dashed circle. F) Gel filtration BRCT in complex with Ab1p, Ab2p, Bach1 and CtIP phosphopeptides at a concentration of 40 μM (1mg/ml). The regions for dimer complex (2:2 complex) and monomer complex (1:1 complex) are high lined in yellow and green shade. Elution positions for void and protein markers Aprotinin (Mw=6500Da), Ribonuclease A (Mw=13700Da), Carbonic anhydrase (Mw=29000Da), Ovalbumin (44000 Da) and Conalbumin (Mw=75000Da) are indicated. G) The molecular weight of BRCT and its complexes with phosphopeptide, measured using native mass spectrometry. H) The native mass spectra of BRCT-Ab1p, BRCT-Ab2p, BRCT-Bach1 and BRCT-CtIP complexes tested at 15 μM. (See also Figure S3)

Figure 4: Mutagenesis studies of the interface of BRCT-Ab2p complex dimer. A) Simplified BRCT-Ab2p dimer interface containing three regions observed in BRCT-Ab2p crystal. B) Detailed interactions mediated though BRCT α1. C) Summary of BRCT and Abraxas mutants. Complexes tested are grouped into four and high-lined in different colours. D) Gel filtration of BRCT and Abraxas mutants. The same colour codes are used as in C. E) Surface representation of BRCA1-1p_short (yellow) and BRCT-Ab2p dimer (blue and pink). Abraxas pS406 binding region is indicated in dashed circle. (See also Figure S4)

Figure 5: Phosphorylation of S404 and S406 are both important for cellular resistance to IR and BRCA1 accumulation at DNA damage sites. A) Generation of Abraxas knockdown U2OS cells complemented with expression of shRNA-resistant HA-tagged wild type, S404A or S406A mutants of Abraxas. B) Increased cellular sensitivity to IR of Abraxas-deficient cells expressing mutants of Abraxas. Colony-survival assay was carried out for cells treated with 4 Gy IR. Data are presented as means ± s.d. Data analyses are processed by ANOVA and statistical significance was determined by Tukey's multiple comparisons test. * $P<0.02$. Three independent experiments were performed. Additional data are presented in Figure S5. C) Representative images of BRCA1 IRIF in Abra1 shRNA knockdown cells complemented with vector, wild-type or mutants of Abraxas in response to 10 Gy IR followed by 2 hr incubation at 37°C. D) The percentage of cells containing more than 10 BRCA1 IRIF foci was quantified. Data are presented as means ± s.d. Data analyses are processed by ANOVA and statistical significance was determined by Tukey's multiple comparisons test. * $P<0.0001$. At least three independent experiments were performed. More than 300 cells were counted for each experiment. Additional data for quantification at different time points post IR are presented in Figure S5. E) Quantification of the intensity of BRCA1 IR induced foci (IRIF). Data are presented as means ± s.d. ($n>50$). Statistical analysis was carried out by Student's t-test. * $P<0.0002$. F) BRCA1 accumulation at damaged chromatin depends on both S404 and S406 residues. Orc2 was used as a marker for chromatin-bound fraction. Cells were treated with 10 Gy IR followed by 2 h incubation at 37°C. Cellular fractionation was carried out and the chromatin fraction was analyzed. (See also Figure S5)

Figure 6. Abraxas promotes BRCA1 BRCT dimerization *in vivo*. A) Abraxas-dependent BRCA1 dimerization *in vivo*. Differentially Myc- and Flag-tagged BRCA1 full-length constructs were transiently transfected into parental 293T (Ctrl) or Abraxas knockout (KO) cells. Lysates from cells treated with 10 Gy IR followed by 1 hr incubation at 37°C were used for Flag-immunoprecipitation. Intensity of individual bands was quantified by densitometric analysis using NIH ImageJ software.

Normalized value (IPed_mycBRCA1/Input_mycBRCA1) was shown in the bar graph. B) Abraxas-dependent BRCA1-BRCT domains dimerization *in vivo*. Differentially Myc- and HA-tagged BRCA1-BRCT domains constructs were transiently transfected into parental 293T (Ctrl) or Abraxas knockout (KO) cells. Lysates from cells treated with 10 Gy IR followed by 1 hr incubation at 37°C were used for HA-immunoprecipitation. Band intensity was quantified with NIH imageJ software. Normalized value (IPed_mycBRCT/Input_mycBRCT) was shown in the bar graph. C) and D) BRCA1 germline mutations F1662S or M1663K decrease BRCA1 dimerization *in vivo*. Myc-tagged BRCA1 full-length (WT-FL) and HA-tagged BRCA1 BRCT (WT-BRCT) or Myc-tagged mutant full-length (F1662S or M1663K) and HA-tagged BRCT triple mutant (TM, F1662S/M1663K/R1670E) were co-expressed in cells. Lysates from cells treated with 10 Gy IR followed by 1 h incubation at 37°C were prepared for either Myc- immunoprecipitation (C) or reciprocal IP with HA- immunoprecipitation (D). Normalized value was shown in the bar graph. E) Abraxas dimerize/oligomerize *in vivo* independent of binding to BRCA1. Differentially tagged GFP- and HA-Flag-tagged wild type (WT) or GFP-tagged and HA-Flag-tagged Abra1 mutants (S404A or S406A) were co-expressed in cells. Anti-GFP immunoprecipitation was carried out with lysates from 293T cells treated or not treated with 10 Gy IR followed by 1 hr incubation at 37°C. The images are from the same blot. F) Abraxas dimerizes/oligomerizes, *in vivo*, through the coiled-coil domain. Immunoprecipitations were carried out with lysates prepared from cells co-expressing HA-Flag-tagged wild-type Abra1 or HA-Flag-tagged coiled-coil domain deletion mutant (ΔCC) and GFP-tagged wild type or ΔCC. (See also Figure S6)

Figure 7. A Model showing IR-induced phosphorylation of Abraxas promotes dimerization of BRCA1 at sites of DNA damage for BRCA1 accumulation and cellular response to IR. In the absence of IR, two BRCA1 bound to BRCA1-A complex do not form stable dimer. Extra phosphorylation at Abraxas S404 induced by IR leads to the final stable dimerization of BRCA1 in the DNA damaged site. The BRCT-Abraxas interaction is indicated in dashed circle for "Pair hugging" interaction model. BRCT domains are represented by grey circles and Abraxas phosphopeptides by pink lines. Line with double arrows indicates interaction for dimerization. P indicates the phosphorylation.

857

858 **Table 1: The statistics of structures**

Crystals	BRCT-Ab1p_short	BRCT-Ab2p
X-ray source	Diamond Light Source Beamline I03	Diamond Light Source Beamline I04-1
Wavelength (Å)	0.9793	0.9200
Space group	$P3_221$	$P2_12_12_1$
Cell dimensions a, b, c (Å) and □□□β, γ (°)	63.8, 63.8, 93.4, 90, 90, 120	86.8, 183.7, 190.5, 90, 90, 90
Resolution (Å)	47.6-2.5	95.3-3.5
[b]R_{sym}	0.051 (0.498) [a]	0.096 (0.701)
I / σ	24 (5.1)	16.4 (2.6)
Wilson B factor	58.6	97.2
Completeness (%)	99.9 (99.8)	99.8 (98.8)
Redundancy	9.3 (9.4)	7.4 (7.8)
Refinement		
Resolution (Å)	47.6-2.5 (2.6-2.5)	95.3-3.5 (3.7-3.5)
No. Unique Reflections	8000	39170
[c]R_{cryst}	0.215 (0.356)	0.235 (0.319)
[d]R_{free}	0.252 (0.374)	0.298 (0.341)
No. Protein atoms	1,701	14,092
No. Copy number of complex in ASU	1	8
Ramachandran favored (%)	97.7	97.1
Average B-factor (Å^2)	66.68	114.6
R.m.s. deviations		
Bond lengths (Å)	0.007	0.007
Bond angles (°)	0.823	0.900

859

860 [a]The statistics in parenthesis are for the highest resolution shell

861 [b]$R_{sym}=\Sigma_h|I_h - \langle I \rangle|/\Sigma_h I_h$, where I_h is the intensity of reflection h, and $\langle I \rangle$ is the mean
862 intensity of all symmetry-related reflections.

863 [c]$R_{cryst}=\Sigma||F_{obs}|-|F_{calc}||/\Sigma|F_{obs}|$, F_{obs} and F_{calc} are observed and calculated structure factor
864 amplitudes.

865 [d]R_{free} as for R_{cryst} using a random subset of the data (about 10% for BRCT-Ab1p_short
866 and 5% for BRCT-Ab2p) excluded from the refinement.
867

868

Figure 1

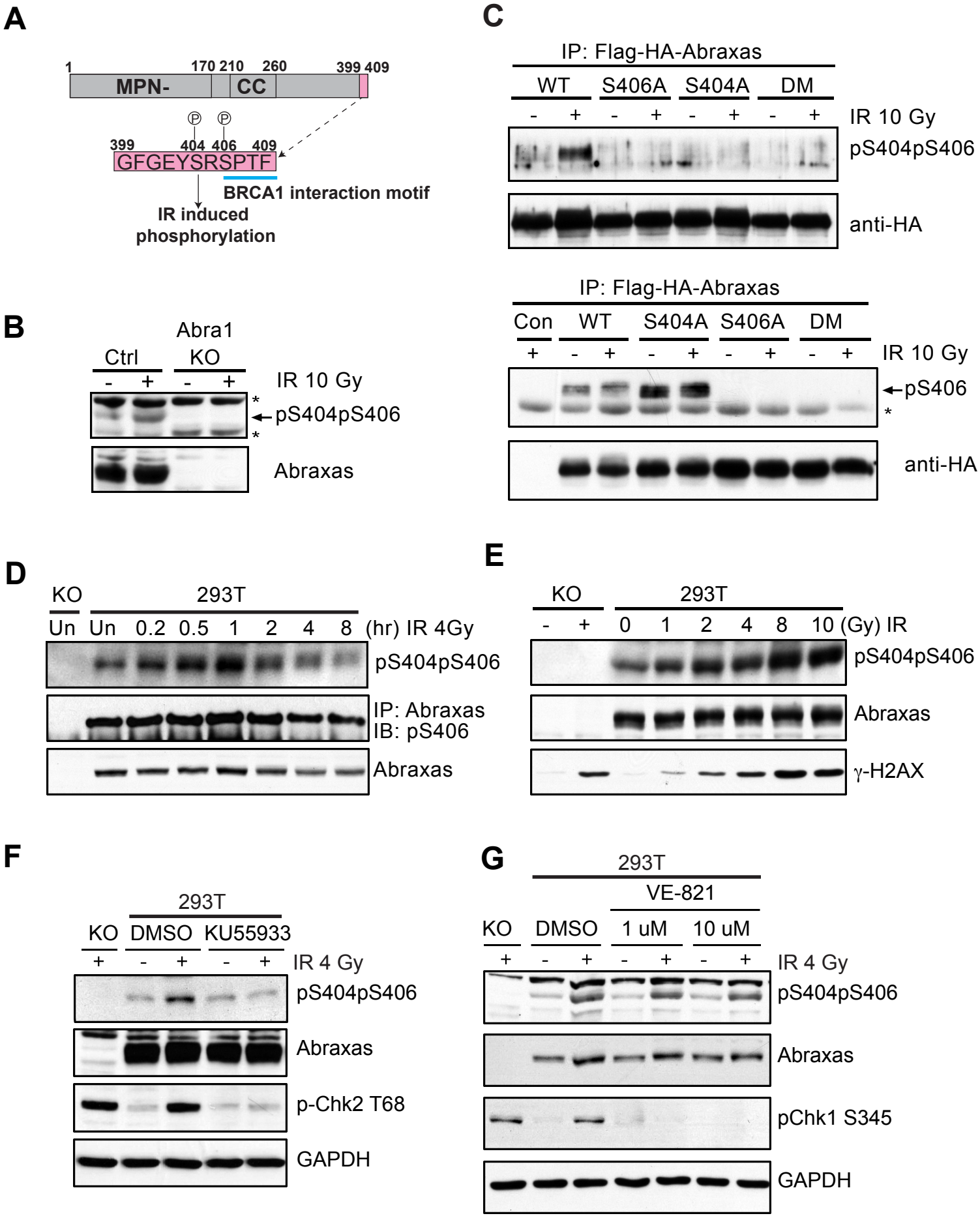
A
1
170 210
260
399 409
MPN-
CC
399
404 406
409
GFGEYSRSPTF
BRCA1 interaction motif
IR induced
phosphorylation
B
Abra1
Ctrl
KO
IR 10 Gy
pS404pS406
Abraxas
C
IP: Flag-HA-Abraxas
WT
S406A
S404A
DM
IR 10 Gy
pS404pS406
anti-HA
IP: Flag-HA-Abraxas
Con
WT
S404A
S406A
DM
IR 10 Gy
pS406
anti-HA
D
KO
293T
Un
0.2
0.5
1
2
4
8
(hr) IR 4Gy
pS404pS406
IP: Abraxas
IB: pS406
Abraxas
E
KO
293T
0
1
2
4
8
10 (Gy) IR
pS404pS406
Abraxas
γ-H2AX
F
293T
KO
DMSO
KU55933
IR 4 Gy
pS404pS406
Abraxas
p-Chk2 T68
GAPDH
G
293T
VE-821
KO
DMSO
1 uM
10 uM
IR 4 Gy
pS404pS406
Abraxas
pChk1 S345
GAPDH

Figure 2

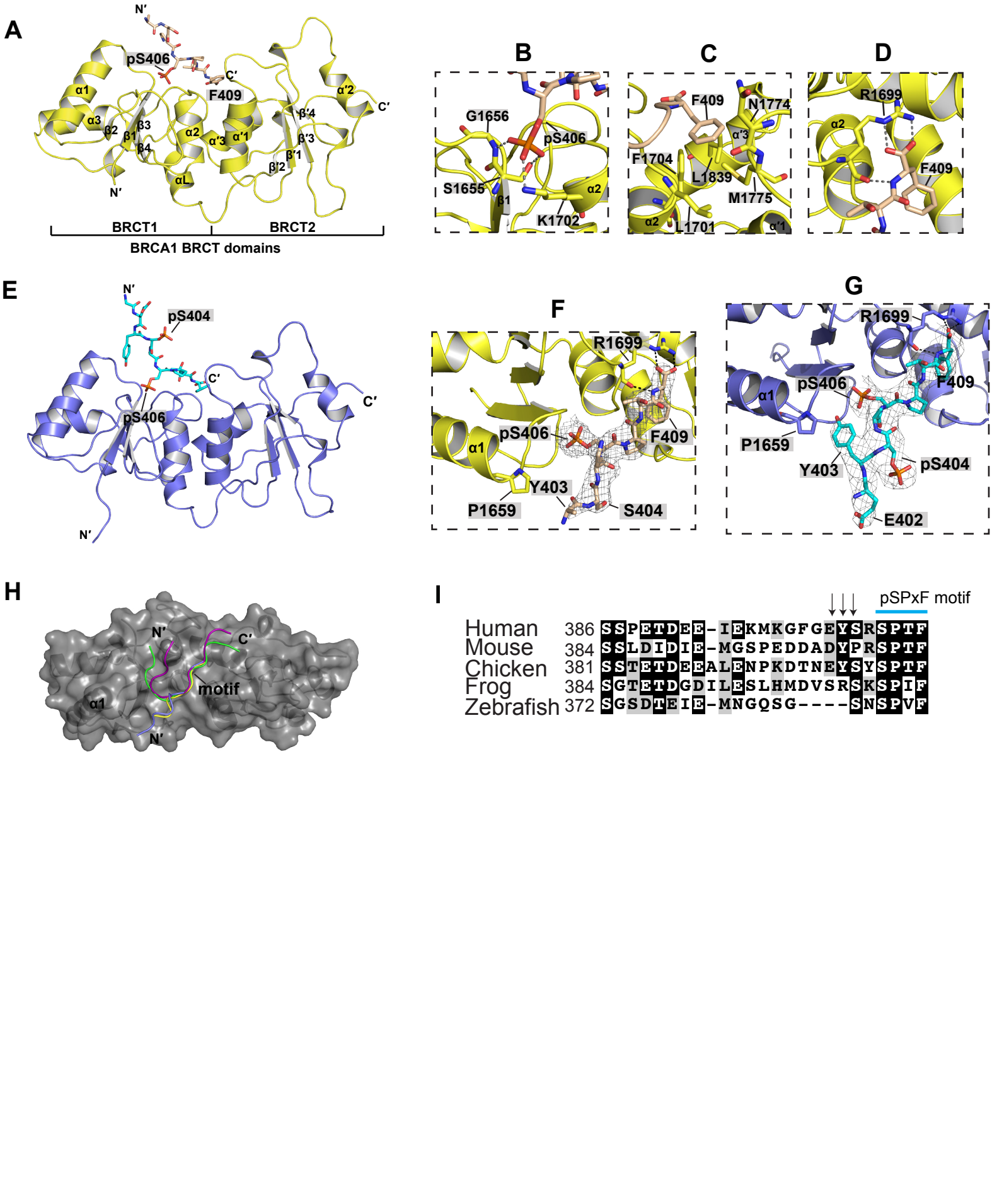
A
N′
pS406
C′
F409
α1
α3
β2
β3
β1
β4
α2
α′3
α′1
α′2
C′
β′4
β′3
β′1
β′2
αL
N′
BRCT1
BRCT2
BRCA1 BRCT domains
B
G1656
pS406
S1655
β1
α2
K1702
C
F409
N1774
α′3
F1704
L1839
M1775
α2
L1701
α′1
D
R1699
α2
F409
E
N′
pS404
C′
C′
pS406
N′
F
R1699
pS406
F409
α1
Y403
P1659
S404
G
R1699
pS406
F409
α1
P1659
Y403
pS404
E402
H
N′
C′
motif
α1
N′
I
pSPxF motif
Human 386 SSPETDEE-IEKMKGFGEYSRSPTF
Mouse 384 SSLDIDIE-MGSPEDDADYPRSPTF
Chicken 381 SSTETDEEALENPKDTNEYSYSPTF
Frog 384 SGTETDGDILESLHMDVSRSKSPIF
Zebrafish 372 SGSDTEIE-MNGQSG----SNSPVF

Figure 3

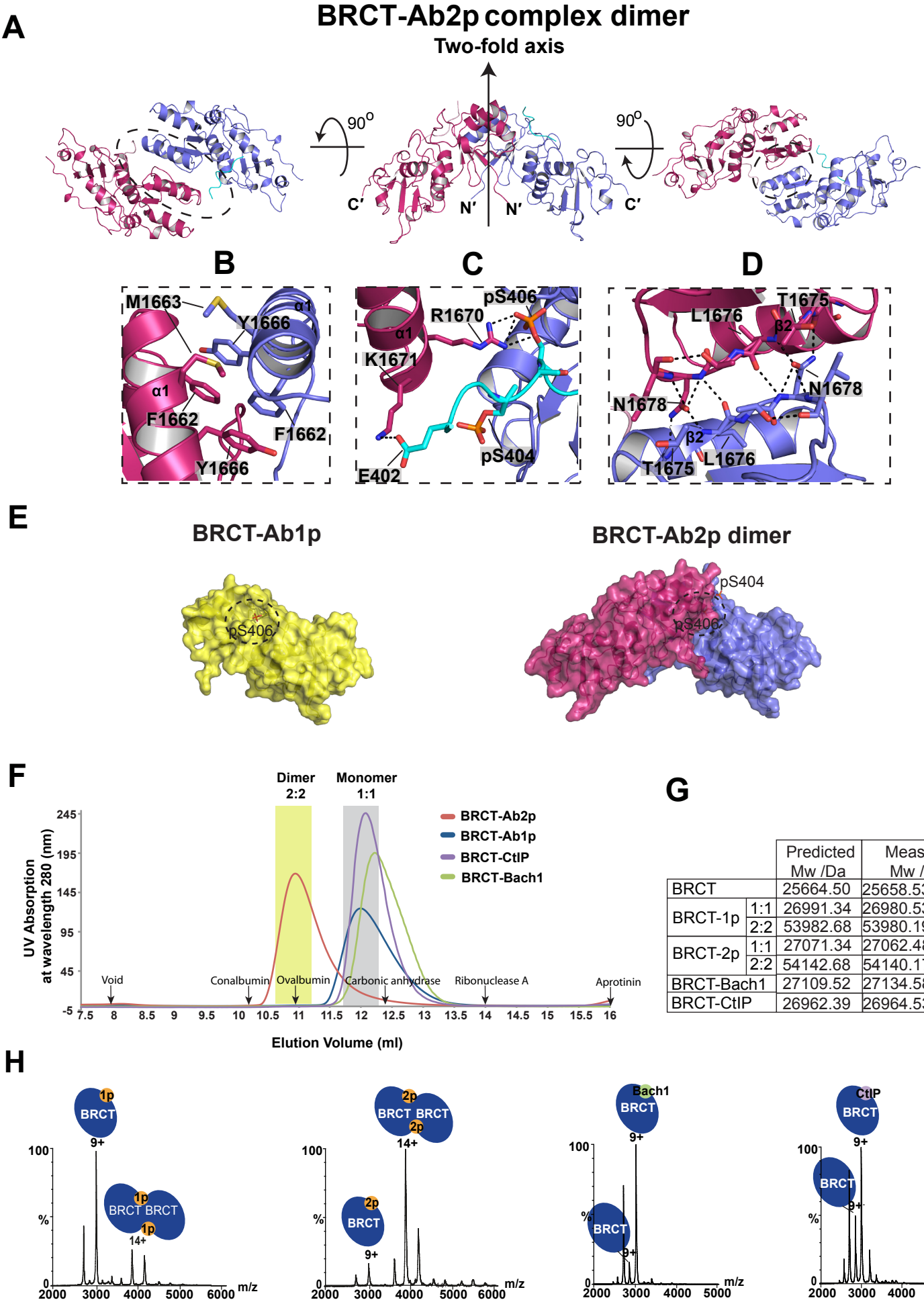

		Predicted Mw /Da	Measured Mw /Da
BRCT		25664.50	25658.53 ±1.62
BRCT-1p	1:1	26991.34	26980.53 ±0.56
	2:2	53982.68	53980.19 ±8.63
BRCT-2p	1:1	27071.34	27062.48 ±0.63
	2:2	54142.68	54140.17 ±19.00
BRCT-Bach1		27109.52	27134.58 ±0.77
BRCT-CtIP		26962.39	26964.53 ±3.39

Figure 4

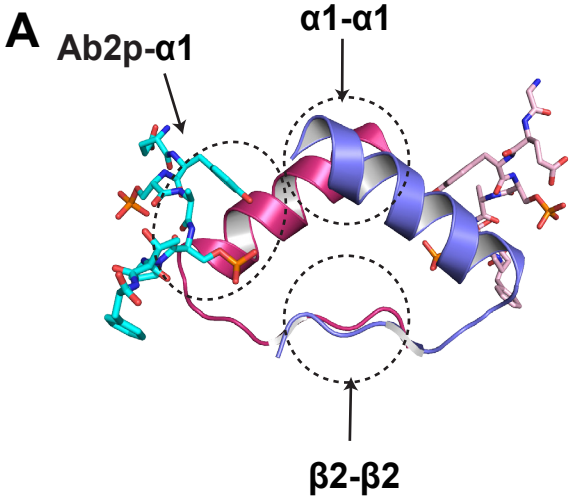

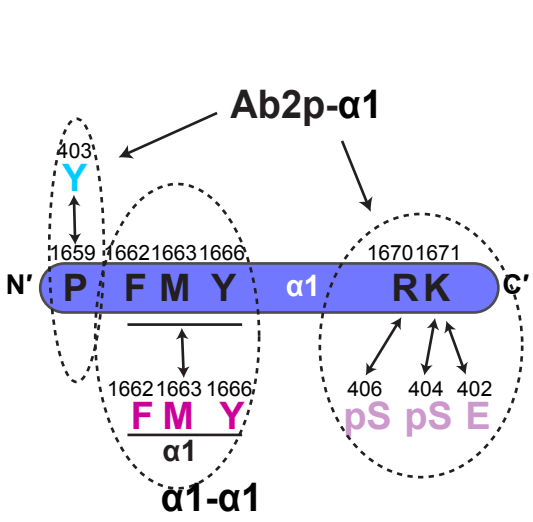

C

	BRCT	Abraxas	
Ab2p-α1	BRCT	Ab2p_short	YpSRpSPTF
	BRCT	Ab1p(S404P)	GFGEYPRpSPTF
	BRCT	Ab1p(S404D)	GFGEYDRpSPTF
	BRCT	Ab2p(F400D)	GDGEYpSRpSPTF
	BRCT	Ab2p(E402R)	GFGRYpSRpSPTF
	R1670E	Ab2p	GFGEYpSRpSPTF
	K1671E	Ab2p	GFGEYpSRpSPTF
	K1671E	Ab2p(E402R)	GFGRYpSRpSPTF
	BRCT	Ab2p(Y403A)	GFGEApSRpSPTF
	BRCT	Ab2p(Y403A)short	ApSRpSPTF
	P1659G	Ab2p(Y403A)	GFGEApSRpSPTF
	P1659G	Ab2p(Y403A)short	ApSRpSPTF
α1-α1	F1662S	Ab2p	GFGEYpSRpSPTF
	M1663K	Ab2p	GFGEYpSRpSPTF
	Y1666A	Ab2p	GFGEYpSRpSPTF
β2-β2	N1678A	Ab2p	GFGEYpSRpSPTF

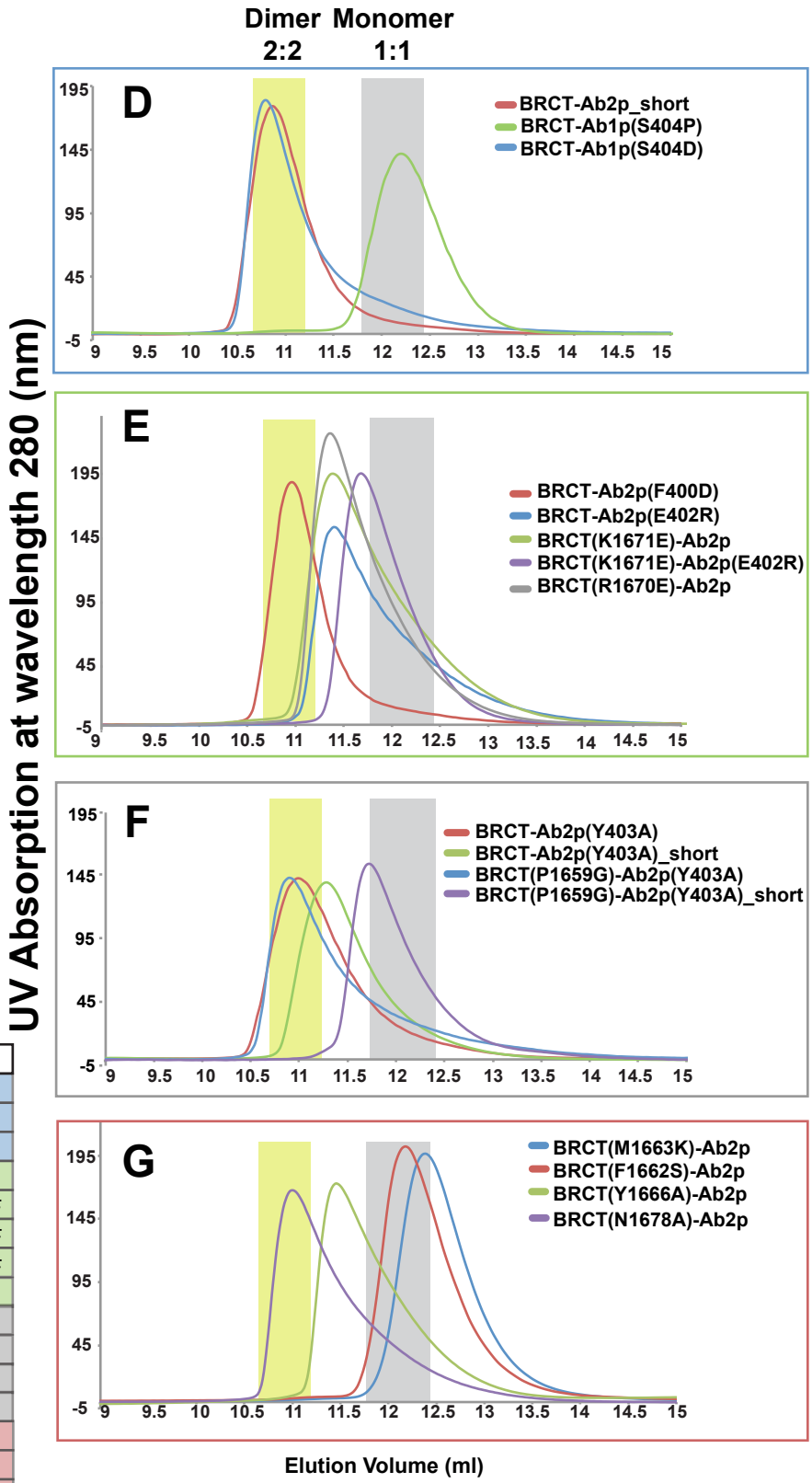

Figure 5

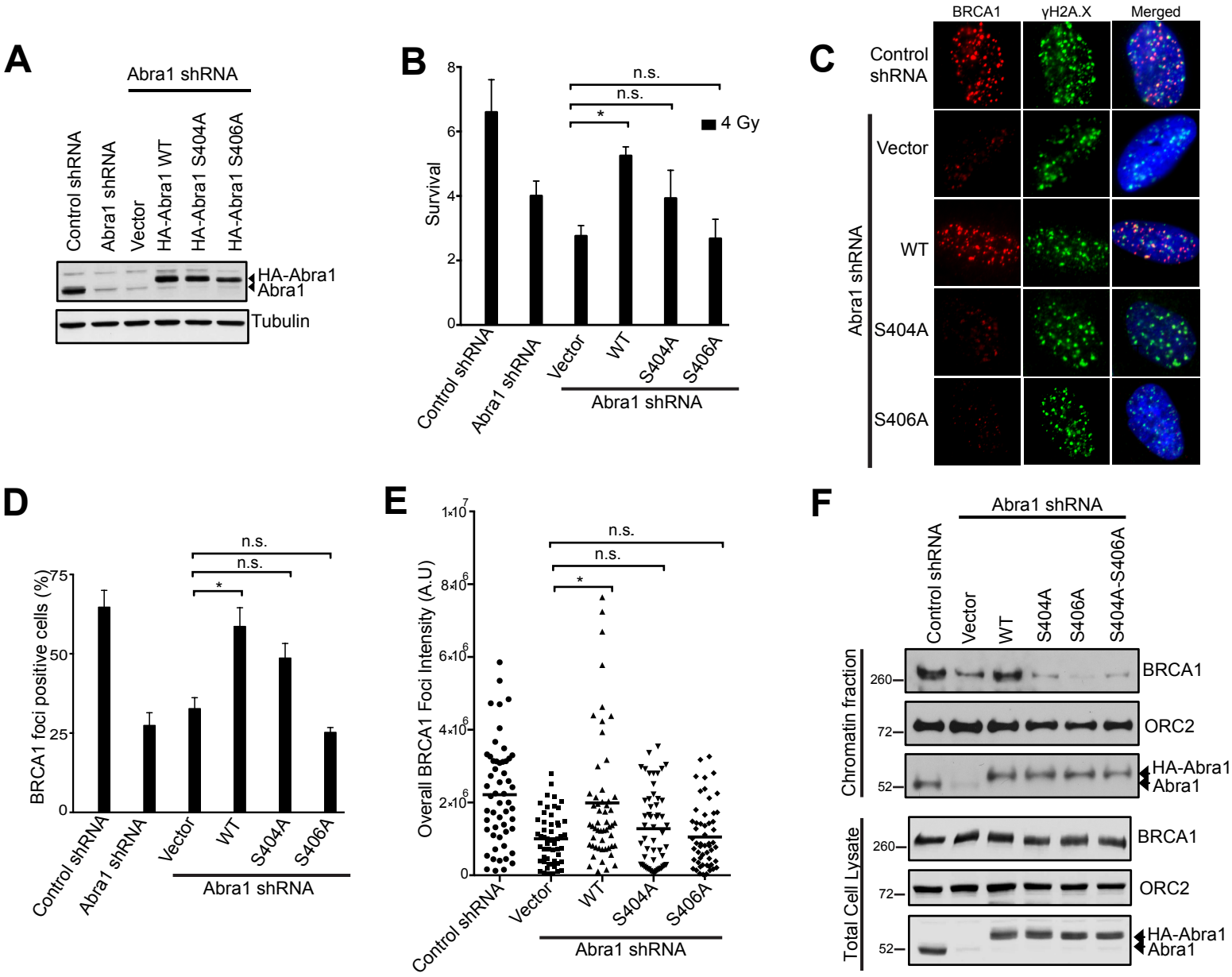
A
Abra1 shRNA
Control shRNA
Abra1 shRNA
Vector
HA-Abra1 WT
HA-Abra1 S404A
HA-Abra1 S406A
HA-Abra1
Abra1
Tubulin
B
Survival
4 Gy
n.s.
n.s.
*
Control shRNA
Abra1 shRNA
Vector
WT
S404A
S406A
Abra1 shRNA
C
BRCA1
γH2A.X
Merged
Control shRNA
Abra1 shRNA
Vector
WT
S404A
S406A
D
BRCA1 foci positive cells (%)
n.s.
n.s.
*
Control shRNA
Abra1 shRNA
Vector
WT
S404A
S406A
Abra1 shRNA
E
Overall BRCA1 Foci Intensity (A.U)
n.s.
n.s.
*
Control shRNA
Vector
WT
S404A
S406A
Abra1 shRNA
F
Abra1 shRNA
Control shRNA
Vector
WT
S404A
S406A
S404A-S406A
Chromatin fraction
BRCA1
ORC2
HA-Abra1
Abra1
Total Cell Lysate
BRCA1
ORC2
HA-Abra1
Abra1

Figure 6

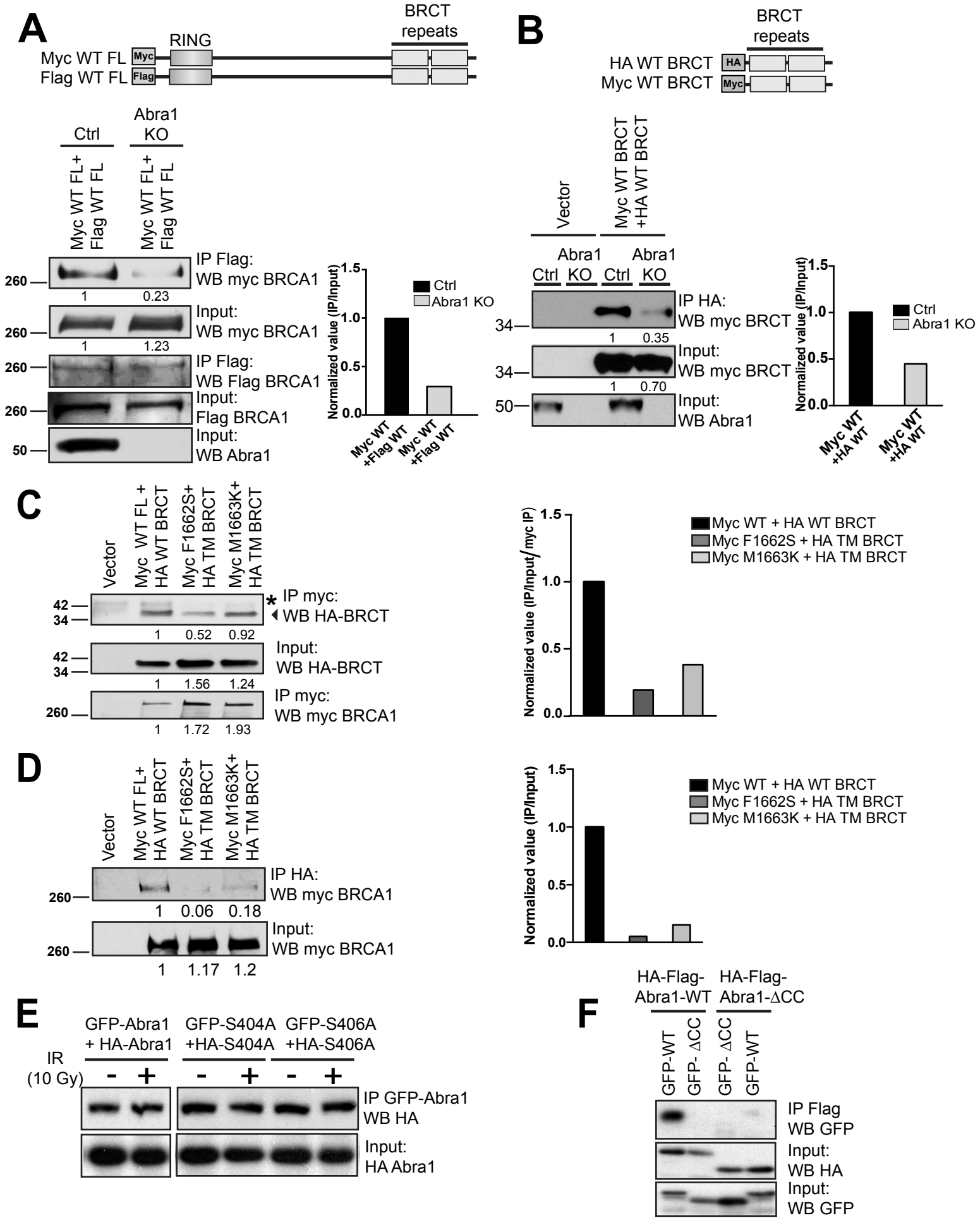
A
RING
BRCT repeats
Myc WT FL
Flag WT FL
Ctrl
Abra1 KO
Myc WT FL+ Flag WT FL
IP Flag: WB myc BRCA1
Input: WB myc BRCA1
IP Flag: WB Flag BRCA1
Input: Flag BRCA1
Input: WB Abra1
Normalized value (IP/Input)
Ctrl
Abra1 KO
Myc WT +Flag WT
B
HA WT BRCT
Myc WT BRCT
Vector
Myc WT BRCT +HA WT BRCT
IP HA: WB myc BRCT
Input: WB myc BRCT
Input: WB Abra1
C
Vector
Myc WT FL + HA WT BRCT
Myc F1662S+ HA TM BRCT
Myc M1663K+ HA TM BRCT
IP myc: WB HA-BRCT
Input: WB HA-BRCT
IP myc: WB myc BRCA1
Normalized value (IP/Input/myc IP)
Myc WT + HA WT BRCT
Myc F1662S + HA TM BRCT
Myc M1663K + HA TM BRCT
D
IP HA: WB myc BRCA1
Input: WB myc BRCA1
E
GFP-Abra1 + HA-Abra1
GFP-S404A +HA-S404A
GFP-S406A +HA-S406A
IR (10 Gy)
IP GFP-Abra1 WB HA
Input: HA Abra1
F
HA-Flag-Abra1-WT
HA-Flag-Abra1-ΔCC
GFP-WT
GFP- ΔCC
IP Flag WB GFP
Input: WB HA
Input: WB GFP

Figure 7

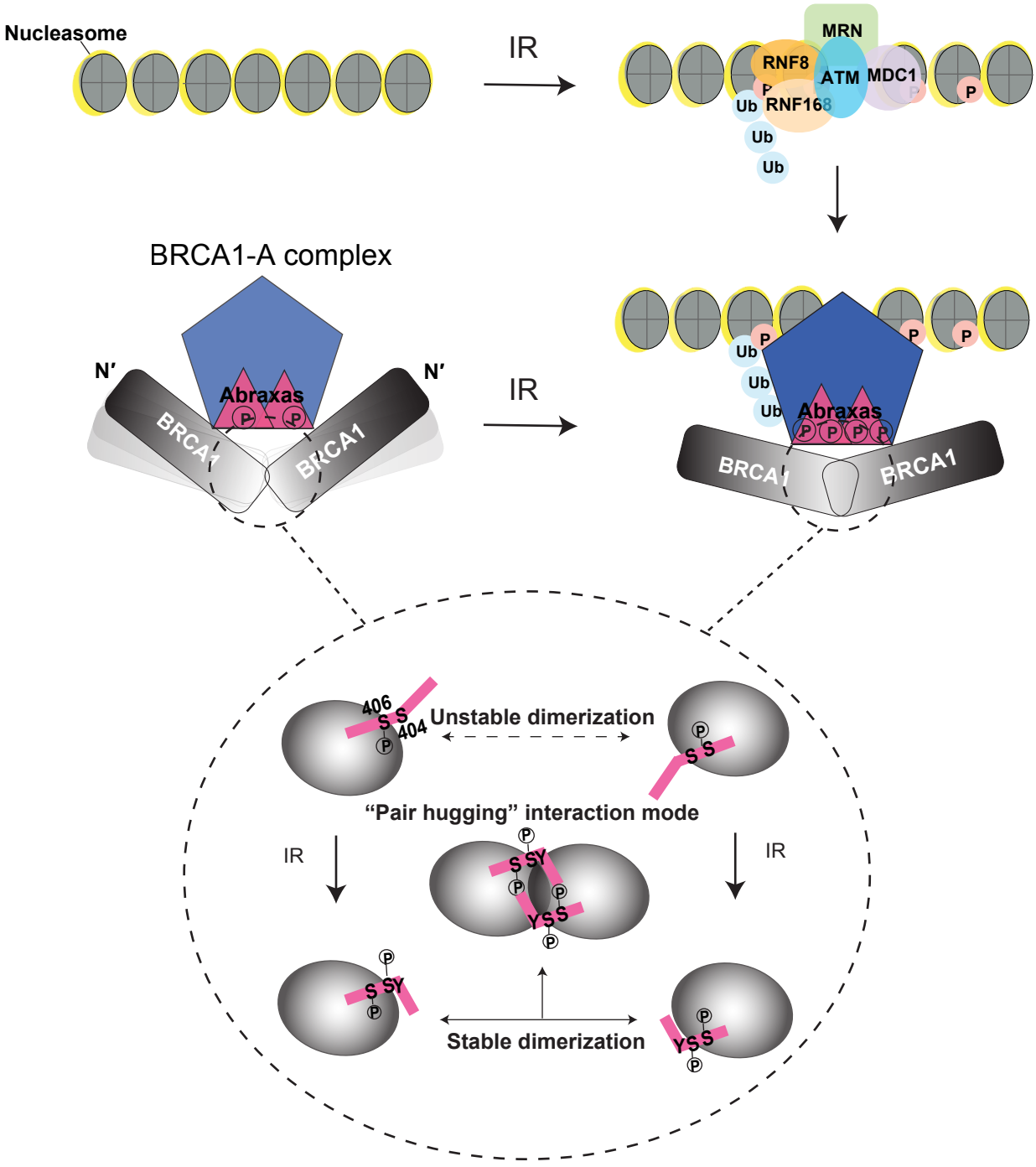
Nucleasome
IR
MRN
RNF8
ATM
MDC1
Ub
RNF168
P
BRCA1-A complex
N'
Abraxas
BRCA1
406
404
Unstable dimerization
"Pair hugging" interaction mode
Stable dimerization

Supplemental Information

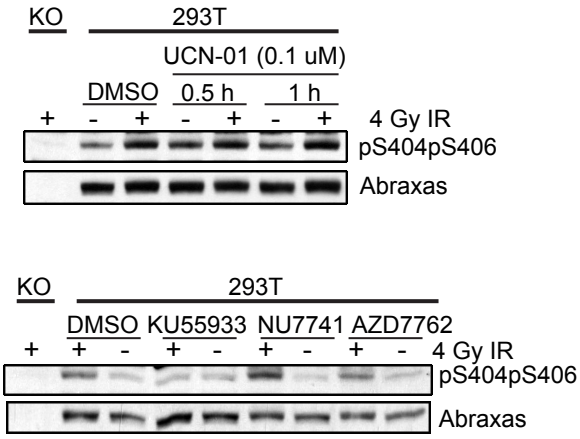

Figure S1 (related to Figure 1): IR-induced double phosphorylation of Abraxas C-terminus S404 and S406 is ATM-dependent, not ATR-, DNAPK-, Chk1- or Chk2 -dependent. Cells were incubated with Chk1 inhibitor (UCN-01), Chk1/2 inhibitor (AZD7762, 10 uM), ATM inhibitor (KU55933, 10 uM), DNA-PK inhibitor (NU7741, 10uM) for 2 hr at indicated concentrations. Cells were then either exposed to 4 Gy IR or untreated followed by 1 hr incubation at 37°C. Abraxas pS404pS406 levels were determined by Western blot.

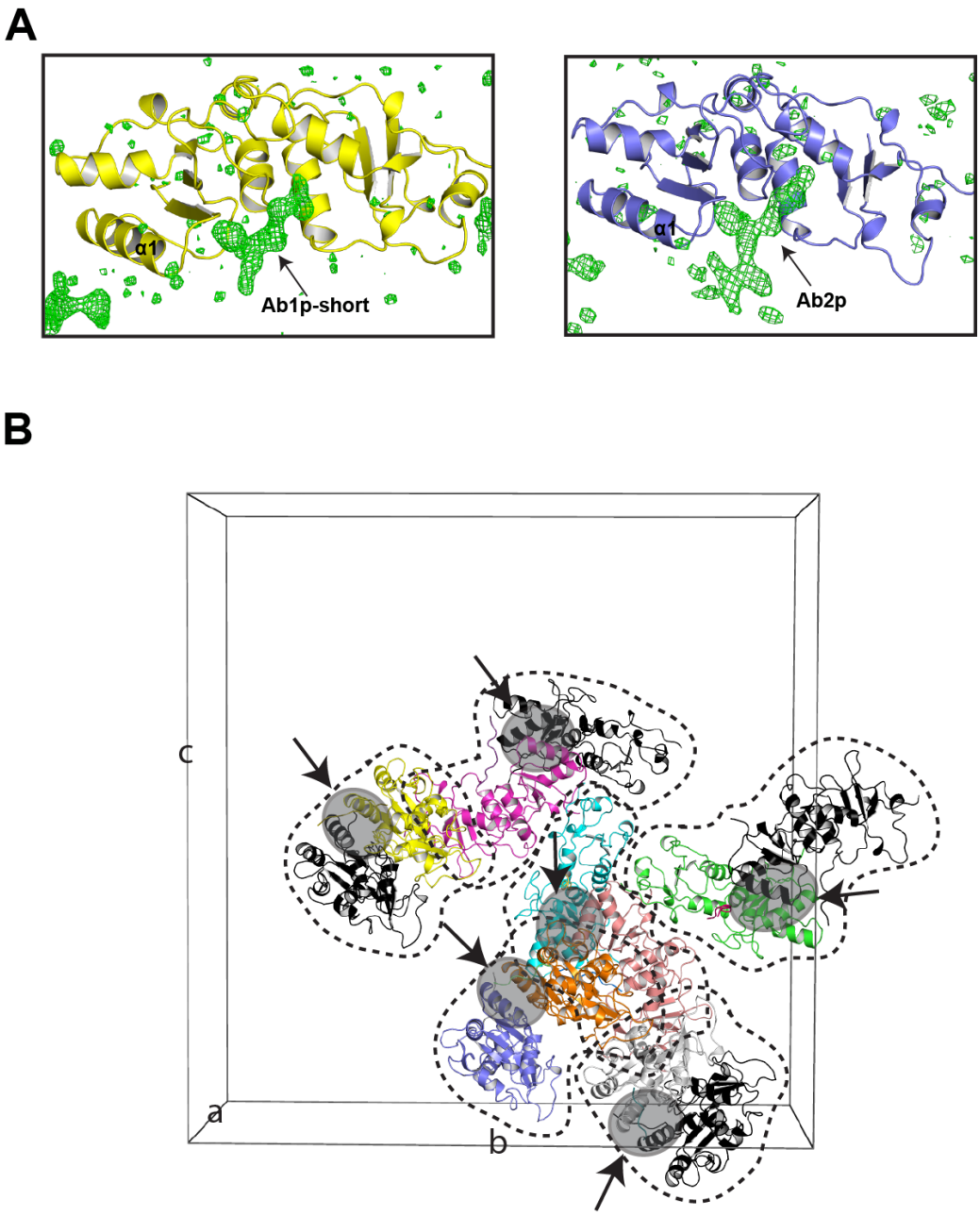

Figure S2 (related to Figures 2 and 3): Electron density for Abraxas phosphopeptide and arrangement of BRCT-Ab2p molecules in the crystal asymmetric unit. A) *Fo-Fc* map (σ=3.0) is shown for Ab1p_short and Ab2p. B) 8 copies of BRCT-Ab2p in one asymmetric unit of the cell (space group $P2_12_12_1$) were coloured in yellow, magenta, cyan, tint, green, orange, blue and grey individually. The same dimer interface occurs in each dimer of the BRCT-Ab2p complex. BRCT-Ab2p molecules belong to different ASUs are coloured in black. Each BRCT-Ab2p complex dimer unit was circulated in dashed line. The dimer interface is highlighted in grey and indicated by a black arrow.

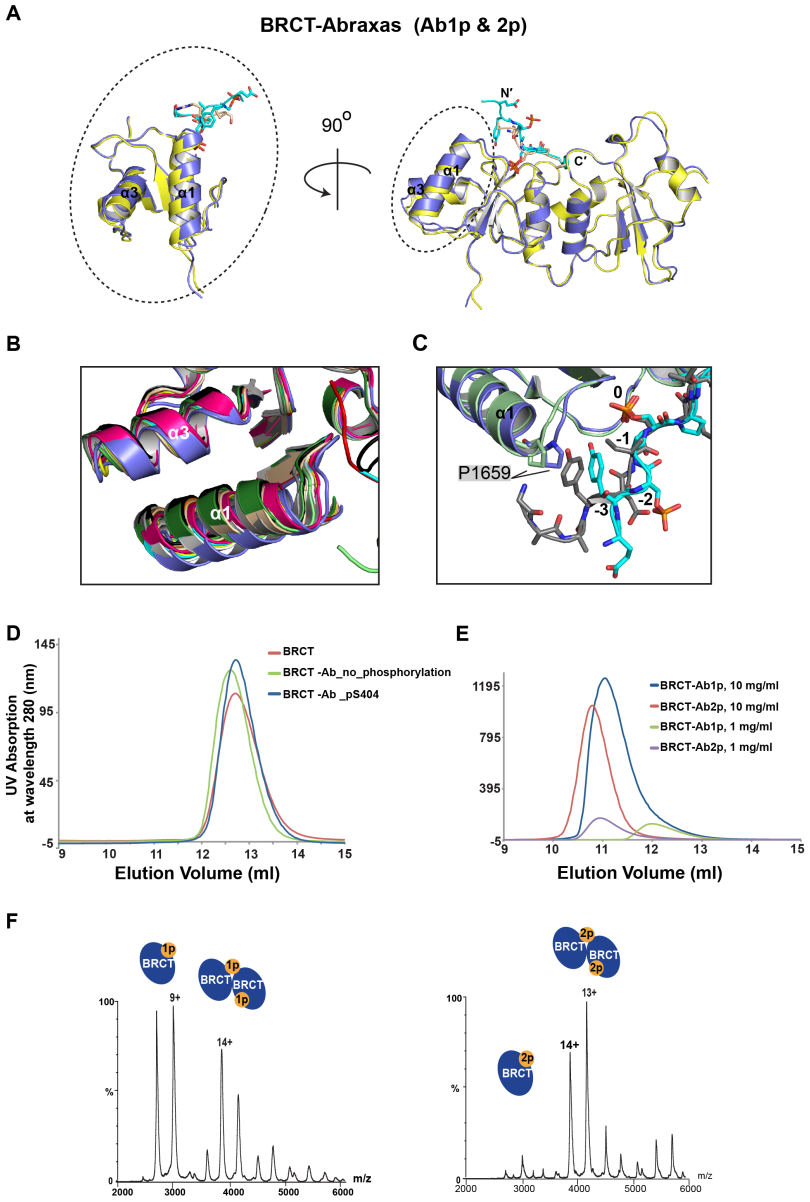

Figure S3 (related to Figure 3): Comparison of BRCT-Abraxas structures with other related BRCA1-BRCT structures, further experiments on the BRCA1-Abraxas complex in solution and native mass spectrometry. A) Superimposition of both BRCT-Ab1p_short (BRCT in yellow and Ab1p_short in wheat colour) and BRCT–Ab2p (BRCT in blue and Ab2p in cyan) structures by aligning the pSPTF motif and the BRCT binding pocket (α2, α1′ and α3′). N- and C-termini are indicated. The black dashed circle highlights the relative structural movements in α 1 and α 3 and is further zoomed in and rotated 90 degrees. B) Superimposition of BRCT-Ab2p with other BRCT related structures: BRCT-Ab2p (blue), BRCT-Ab1p_short (yellow), BRCT-Bach1 (PDB: 1T15 (cyan) and 1T29 (red) (Clapperton et al., 2004; Shiozaki et al., 2004), BRCT with tetrapeptide motifs (PDB: 3K0K (orange) and 3K0H (wheat)) (Campbell et al., 2010), BRCT with acetyl-coA carboxylase 1 peptide (PDB:3COJ (pink)) (Shen and Tong, 2008) , BRCT-CtIP (PDB: 1Y98 (black)) (Varma et al., 2005), ATRIP (PDB: 4IGK (dark green)) (Liu and Ladias, 2013), optimized peptide (PDB:1T2V (light green)) (Williams et al., 2004) and BAAT1 (PDB:4IFI (white)) (Liu and Ladias, 2013). C) Superimposition of BRCT-Ab2p with BRCT-Optimized peptide (PDB code: 1T2V). The positions of related residues are relative to the phosphorylated serine in pSxxF is in the 0 position. D) Elution profile of BRCT only, BRCT-Ab_no_phosphorylation and BRCT-Ab pS404 are superimposed. BRCT, BRCT-Ab_pS404 and BRCT-Ab_no_phosphorylation are eluted at similar positions. E) BRCT-Ab1p and BRCT-Ab2p at high concentration (10 mg/ml). **(**F) Native mass spectra of BRCT-Abraxas complexes. Protein samples are tested at 75 μM concentration.

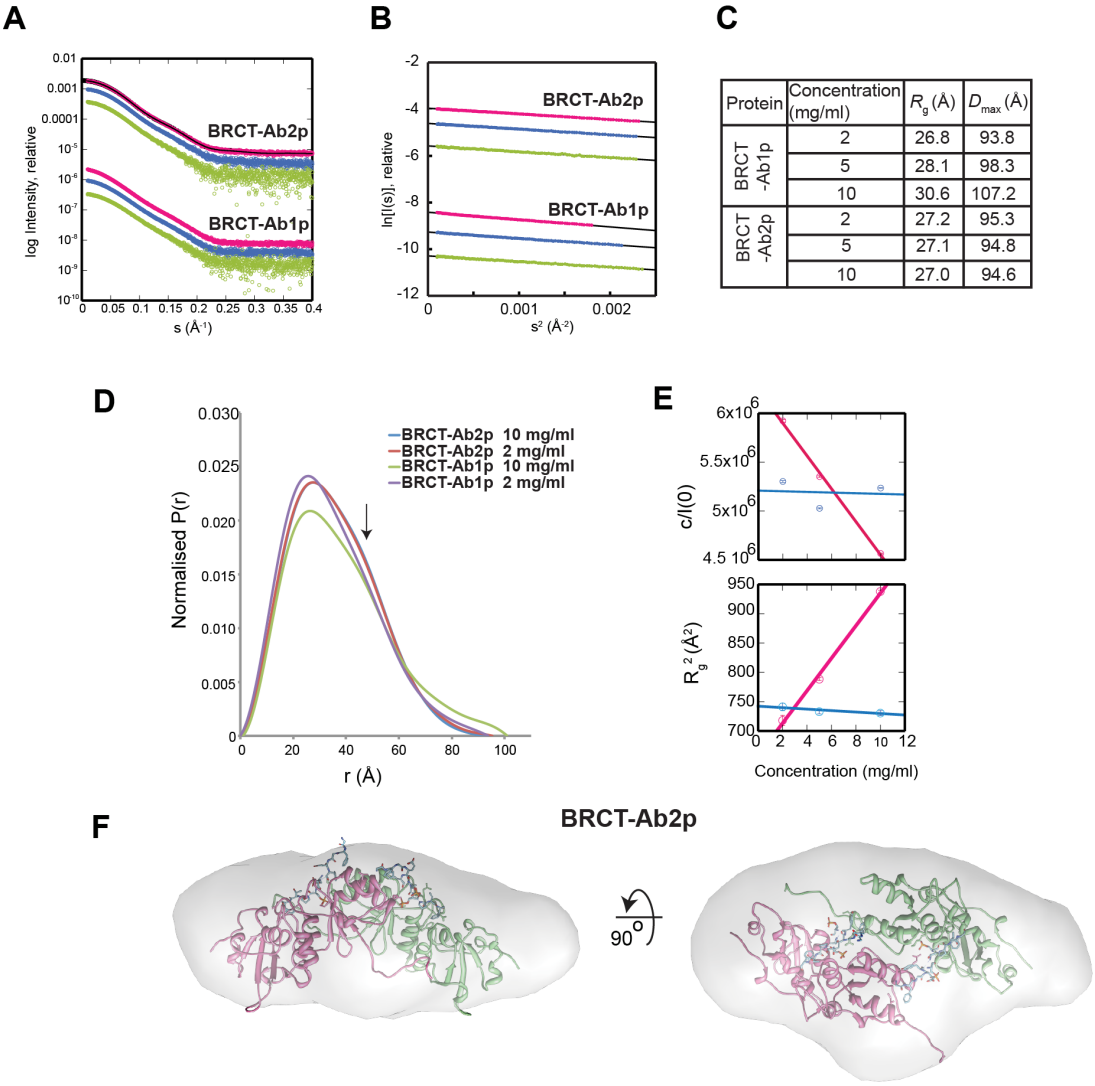

Protein	Concentration (mg/ml)	R_g (Å)	D_{max} (Å)
BRCT-Ab1p	2	26.8	93.8
	5	28.1	98.3
	10	30.6	107.2
BRCT-Ab2p	2	27.2	95.3
	5	27.1	94.8
	10	27.0	94.6

Figure S4 (related to Figure 4). Identification of BRCT-Abraxas using SAXS. A) The SAXS scattering profiles of BRCT-Ab2p at 2 mg/ml (green), 5 mg/ml (blue) and 10 mg/ml (pink) are shifted up compared to those of BRCT-Ab1p for clarity. The black line is simulated-scattering profiles of the crystal structure of BRCT-Ab2p 2:2 dimer complex. B) Guinier plots of BRCT-Ab1p and BRCT-Ab2p. The scattering data (dot; s<1.3/R_g) are shown together with linear fit lines (black). C) R_g and D_{max} values of BRCT-Ab1p and BRCT-Ab2p. D) Pairwise distance-distribution functions of BRCT domains. The distribution functions of BRCT-Ab1p at 2 mg/ml (green) and 10 mg/ml (purple) are shown together with that of BRCT-Ab2p 2 mg/ml (red) and BRCT-Ab2p 10 mg/ml (blue). Each distribution function was normalized so that its total area value is 1. E) Concentration dependence of $I(0)$ and radius of gyration R_g of BRCT-Ab1p (pink) and BRCT-Ab2p (blue). The top panel shows the plots of the concentration c versus $c/I(0)$. The lower panel shows the plots of c versus the square of R_g. The top and lower panels share the same abscissa axis. BRCT-Ab1p and BRCT-Ab2p are represented by pink and blue respectively. F) Shape reconstruction of BRCT-Ab2p. The structure of BRCT-Ab2p dimer, of which N-termini were modeled using RapperTK, were fitted in the averaged DAMMIN envelope.

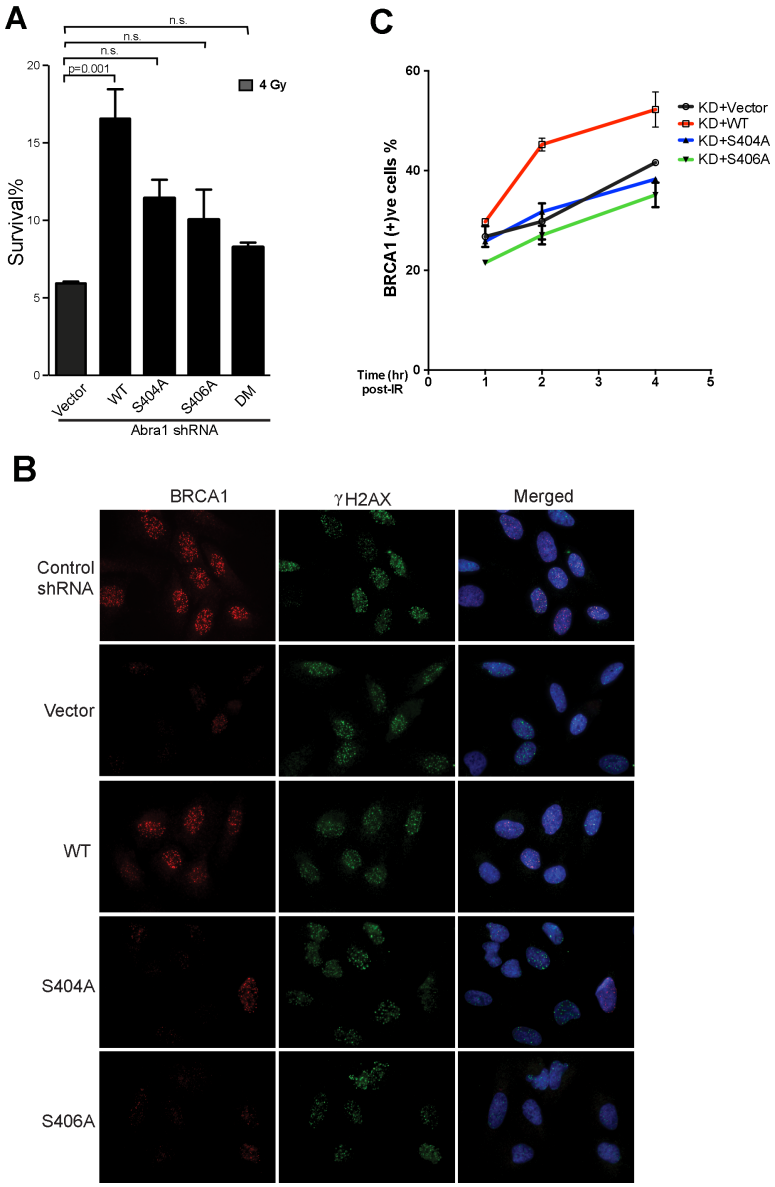

Figure S5 (related to Figure 5): Phosphorylation of S404 and S406 are both important for cellular resistance to IR and BRCA1 accumulation at DNA damage sites. A) An independent colony survival assay for Abraxas-deficient cells expressing WT or mutants of Abraxas treated with 4 Gy IR. Data are presented as means ± s.d. Data analyses are processed by ANOVA and statistical significance was determined by Tukey's multiple comparisons test. B) Representative images of BRCA1 IRIF in Abra1 shRNA knockdown cells complemented with vector, wild-type or mutants of Abraxas in response to 10 Gy IR followed by 2 hr incubation at 37°C. C) Quantification of the percentage of cells containing more than 10 BRCA1 IRIF foci at indicated time points after 10 Gy IR followed by incubation at 37°C. More than 300 cells were counted for each experiment.

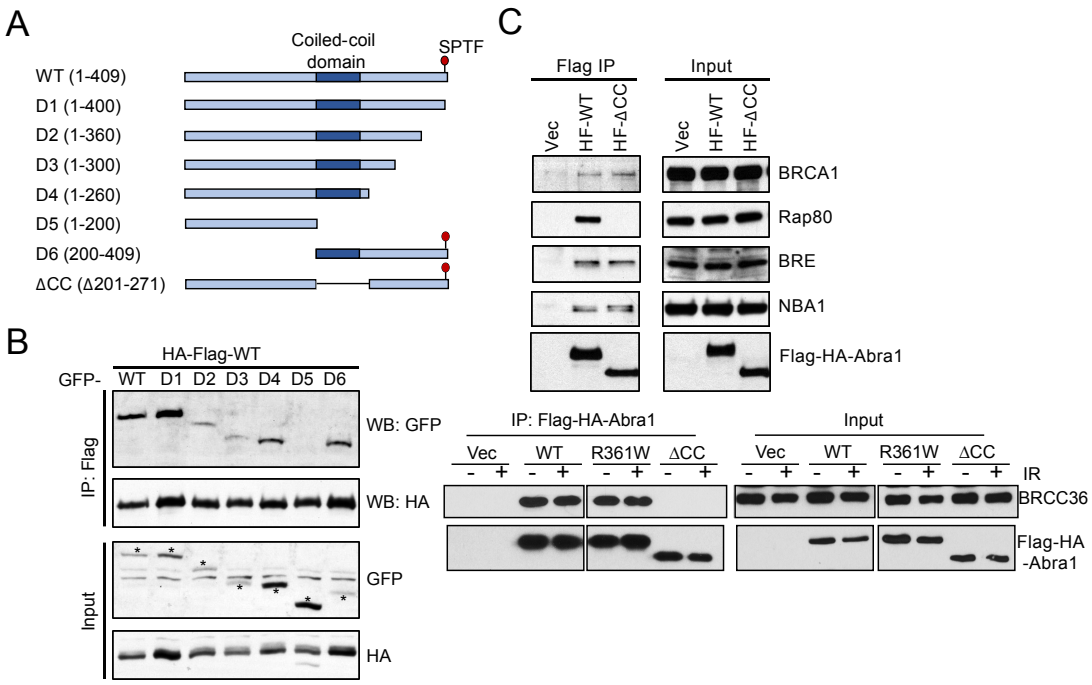

Figure S6 (related to Figure 6): Abraxas forms dimers through the coiled-coil domain independent of binding to BRCA1. A) A schematic view of the Abraxas deletion mutants generated. B) The coiled-coil domain is required for Abraxas dimerization. HA-Flag-tagged wild type (WT) Abraxas were co-transfected with GFP-tagged WT or deletion mutants of Abraxas into 293T cells. 48 h after transfection, cell lysates were prepared and used for Flag-immunoprecipitation. Western blots with GFP or HA antibodies are shown. Expression of GFP-tagged WT or mutant-Abraxas protein products are indicated with "*". C) Abraxas coiled-coil deletion mutant (**Δ**CC) retains interaction with other components of the BRCA1-A complex. HA-Flag-tagged WT or **Δ**CC were transiently expressed in 293T cells. The samples in the upper panel were prepared from cells not treated with ionizing radiation. The lower panel shows the interaction of Abraxas with BRCC36. An Abraxas mutant (R361W) that retains the interaction with BRCC36 was also used as a control. Samples of cells treated with 10 Gy IR or untreated were used to show the interaction of Abraxas with BRCC36. Flag-immunoprecipitation was carried out followed by Western blots with antibodies against indicated protein.

Supplemental Experimental Procedures

Cell Lines, Cell Culture and Antibodies

To generate Abraxas knockdown cells, U2OS cells were infected with retrovirus containing shRNAs against Abraxas followed by selection with puromycin (0.8 ug/ml) for 5 days. The Abraxas knockdown stable cell line was then complemented with expression of empty MSCV vector or expression constructs containing HA-tagged WT or mutant Abraxas, and selected with Blasticidin (9 ug/ml) 1 week for stable expression. 293T Abraxas knockout cells were generated by CRISPR-Cas9 system (Fu et al., 2014; Ran et al., 2013) In brief, 293T cells were infected with lentivirus carrying pLentiCRISPR including Cas9 and sgRNA, which targets Abraxas genomic sequence 5'-GGCGGCGGTAGCATGGA-3'. Cells were then subjected to puromycin selection (2 ug/ml) for three days and plated in low density for culturing for ten days. Single colonies were selected and knockout cells were confirmed by Western blotting with Abraxas antibody and PCR-sequence of the Abraxas genomic locus. Rabbit anti-Abraxas double-phosphorylated pS404pS406 antibody was generated using conjugated GFGEYpSRpSPTF phosphopeptide. The rabbit anti-Abraxas and anti-Abraxas S406 antibodies were generated as previously described (Wang et al., 2007). Other antibodies used were BRCA1 antibodies (D9, Santa Cruz Biotechnologies); GFP antibodies (Invitrogen); γ-tubulin antibodies (Sigma); rabbit anti-HA antibodies (Cell Signaling), Rabbit γH2AX (Upstate), Orc2 (PharMingen).

Immunofluorescence

Abra1 shRNA knockdown cells complemented with empty vector, wild type or mutants of Abra1 were analyzed for BRCA1 IR-induced foci formation (IRIF). At least 500 cells were counted for each cell type and cells containing more than 10 foci were counted as positive. Mean and standard deviations are shown in the Figures 5B,D,E, S5A and statistical analysis was performed by student's t-test or ANOVA with Tukey's multiple comparisons test. p-value is as indicated. All images were obtained with a Nikon TE2000 inverted microscope with a Photometrics Cool- Snap HQ camera. Quantification of BRCA1 was performed using Imaris software (Bitplane). The DAPI channel was used to select the nuclei of the cells in the field, red and green channel were used for BRCA1 and γH2AX, respectively. For BRCA1 foci intensity measurement, foci were defined as particles bigger than 0.25 μM in diameter with an intensity cut-off value (1200) to eliminate background. At least 50 cells were counted and plotted using GraphPad Prism software.

Cell Lysis and Immunoprecipitation

Cells were lysed in NETN buffer (50 mM Tris-HCl, pH 8.0, 150 mM NaCl, 1 mM EDTA, 0.5% Nonidet P-40) with protease inhibitors and protein phosphatase inhibitors, 1 mM NaF, and 1 mM Na_3VO_4. For Flag IP, cell lysates were incubated with Flag beads (Sigma) overnight with gentle agitation at 4^{o}C. The beads were washed with NETN lysis buffer four times and eluted with 3X sample buffer for Western blot analysis. For analyzing Abraxas dimerization *in vivo*, GFP-tagged and HF-tagged Abraxas wildtype, S404A, S406A mutant or coiled-coil deletion mutant were transiently transfected to 293T cells. Two days after transfection, cells were either untreated or exposed to 10 Gy IR. 2 hr later, cells were collected for GFP- or Flag- IP and Western blot was probed with either antibodies against HA or GFP. For analyzing BRCA1 dimerization *in vivo*, Flag- or Myc-tagged BRCA1 full-length wild type or mutants, or HA- and Myc-tagged BRCA1 BRCT fragments were analyzed in a similar way. ATM inhibitor (KU55933), ATR inhibitor (VE-821), DNA-PK inhibitor (NU7441) and Chk1/2 inhibitor (AZD7762) were purchased from Selleckchem and dissolved in dimethyl sulphoxide (DMSO).

Clonogenic Survival Assay

Abra1 shRNA knockdown cells complemented with empty vector, wild type or mutants of Abra1 were analyzed for cell survival in response to IR. Stable U2OS cell lines were seeded at low density in 10 cm dishes and irradiated with 4 Gy ionizing irradiation using a ^{137}Cs source. The cells were then cultured at 37°C for 14 days to allow colonies to form. Colonies were stained with 2% methylene blue and 50% ethanol for 10 min. Colonies containing 50 or more cells were counted as positive and statistical data were analyzed by analysis of variance (ANOVA) with Tukey's multiple comparisons test.

Chromatin fractionation

Cells were irradiated at 10 Gy followed by 1 hr incubation at 37^{o}C. For total cell extracts, cells were lysed in NETN150 buffer containing protease inhibitor mixture and analyzed by Western blot. For

chromatin fractionation, irradiated cells were washed in PBS and resuspended in Buffer A (10 mM Hepes pH 7.9, 10 mM KCl, 1.5 mM $MgCl_2$, 0.34 M sucrose, 10% glycerol, 5 mM NaF, 1 mM Na_3VO_4 , 1 mM dithiothreitol (DTT), and protease inhibitor mixture) containing 0.1% Triton X-100, and incubated on ice for 5 min for permeabilization. The cytosolic fraction was then separated by centrifugation at 4000 rpm for 5 min at 4°C. The supernatant was discarded and the nuclei pellet was washed once with Buffer A and resuspended in Buffer B (3 mM EDTA, 0.2 mM EGTA, 1 mM DTT, protease inhibitor mixture) and incubated for 30 min on ice. The soluble nuclear fraction was separated by centrifugation at 4500 rpm for 5 min. The chromatin fraction pellet was washed with Buffer B and resuspended in 100 µl Laemmli sample buffer and sonicated for 10 sec before analysis.

BRCT constructs, expression and purification

The BRCT domains (residues 1646-1859) of the *BRCA1* gene were amplified from IMAGE cDNA (ID 7961446) using PCR and cloned into the pHAT2 vector (with noncleavable N-terminal His-tag) (Peränen et al., 1996) and transformed into Rosetta^{TM}2 (DE3) cells (Invitrogen). Cell culture was grown in LB medium till the OD_{600} was approximately 0.6. IPTG was added to a final concentration of 1 mM and cells were grown overnight at 16^{o}C. 1 g of harvested cells was resuspended with 10 ml of lysis buffer (50 mM Tris pH 8.0, 300 mM NaCl, 20 mM imidazole and one protease inhibitor tablet per 50 ml lysis buffer). Cells were lysed using sonication. The supernatant after centrifugation was then filtered by 0.45 µm filter and loaded onto HisTrap HP 5ml (GE healthcare) pre-equilibrated with binding buffer (50 mM Tris pH 8.0, 300 mM NaCl and 20 mM imidazole) After washing with 10x column volume of binding buffer and binding buffer with 50 mM imidazole, the protein was eluted using elution buffer (50 mM Tris pH 8.0, 300 mM NaCl and 200 mM imidazole). The eluted BRCT domains were about 80% pure as assessed by 12% SDS-PAGE. Remaining contaminants were removed by gel filtration using a Superdex 75 10/300 equilibrated with Buffer A (20 mM Tris pH 8.0, 150 mM NaCl and 5 mM DTT). Fractions containing pure BRCT sample were analyzed in 12% SDS-PAGE gel, pooled, concentrated and stored at -80^{o}C. All mutants were made by site-directed mutagenesis using wt BRCT in pHAT2 as PCR template. Mutant proteins were expressed and purified using the procedure described above.

Phosphopeptides

All phosphopeptides were synthesized to above 95% purity without modification at both N and C terminus (Biomatik). Peptides were dissolved in Buffer A to 25 mg/ml. The pH of the peptide solution was adjusted to near pH 8 using 0.5 M NaOH. The peptide names and sequences are listed below:
Abraxas peptides: 1)Ab1p: GFGEYSRpSPTF; 2)Ab2p: GFGEYpSRpSPTF; 3)Ab1p_short: YSRpSPTF; 4)Ab2p_short: YpSRpSPTF; 5)Ab_pS404: GFGEYpSRSPTF; 6)Ab_no_phosphorylation: GFGEYSRSPTF; 7)Ab2p(Y403A): GFGEApSRpSPTF; 8)Ab2p(Y403A)_short: ApSRpSPTF; 9)Ab2p(F400D): GDGEYpSRpSPTF; 10)Ab2p(E402R): GFGRYpSRpSPTF; 11)Ab1p(S404P): GFGEYPRpSPTF; 12)Ab1p(S404D): GFGEYDRpSPTF; 13)Bach1: ISRSTpSPTFNKQ; 14) CtIP: PTRVSpSPVFGAT

Protein crystallization and data collection

Crystals were cryoprotected in crystallization solution containing 30% glycerol using the two-step transferring method and then subsequently flash frozen in liquid nitrogen. The structure of BRCT-Bach1 (PDB code 1T15) (Clapperton et al., 2004) without Bach1 phosphopeptide was used as the search model. Relaxed NCS restraints among all the molecules of the BRCT-Ab2p in the asymmetric unit were used in the refinement protocol as defined in phaser_refine module. This resulted in clear $2F_o$-F_c and F_o-F_c electron density that allowed manual building of the Abraxas peptide using *Coot* (Emsley et al., 2010) (Figure S1). For BRCT-Ab2p, the structure connectivity and disordered region vary among molecules in the ASU depending on its position in the crystallographic packing, therefore chains IDs G, H, O and P have poorer electron density map than other chains. Further structure refinements also included simulated annealing, optimizing X-ray/Stereochemistry weight, optimizing X-ray/ADP weight and side chain adjustment using *Coot*. The buried surface area after dimerization of BRCT-Ab2p was calculated using PISA (Krissinel and Henrick, 2007).

Identification of BRCT-Ab1p and BRCT-Ab2p using SAXS

We carried out SAXS of the BRCT-Ab1p and BRCT-Ab2p in different concentrations. The scattering profiles (Figure S4A) of BRCT-Ab1p and BRCT-Ab2p at high concentration (10 mg/ml) were similar and indicated that the samples were monodisperse (Figure S4B). The scattering profiles of BRCT-Ab2p did not change by increasing the concentration of the sample whereas BRCT-Ab1p changed particularly at low angle. We then used the BRCT-Ab2p dimer crystal structure to calculate its

scattering profile and compare it with the observed profile of BRCT-Ab2p (black line in Figure S4A). The calculated-scattering profiles of the 2:2 BRCT-Ab2p dimer explain the observed scattering profiles much better than for the 1:1 complex (χ=1.675 and 3.806 respectively) indicating that BRCT-Ab2p is dimerized in solution. The fitting of the 2:2 dimer structure against the scattering profile of BRCT-Ab1p was better at 10 mg/ml (χ=1.934) than at 2 mg/ml (χ=5.975). The pairwise distance-distribution functions of BRCT-Abraxas complexes showed that BRCT-Ab2p has a very similar profile at both 10 mg/ml and 2 mg/ml concentrations. They both have a shoulder around 50 Å (indicated by black arrow in Figure S4D), which is clearer than that of BRCT-Ab1p at 10 mg/ml and 2 mg/ml. Furthermore, BRCT-Ab1p showed inter-particle attraction by increasing the concentration of the sample but BRCT-Ab2p did not (Figure S4E) (Nakasako et al., 2005). BRCT-Ab2p complex dimer crystal structure can be fitted into the envelope of an averaged DAMMIN model of the dimer (Figure S4F).

SAXS analysis

SAXS data of 2, 5 and 10 mg/ml BRCT-Ab1p and BRCT-Ab2p in Buffer A (20 mM Tris pH 8.0, 150 mM NaCl and 5 mM DTT) were collected at I22 in Diamond Light Source. Protein samples were loaded into glass capillaries using a BIOSAXS robot and the scattering intensities of the sample were measured at 5^{o}C using the Pilatus 2M detector. The scattering vector s is $4\pi\sin\theta/\lambda$, where θ is half of the scattering angle and λ is the wavelength (0.9987 Å). Data reduction was carried out using DAWN. Primus was used to interpolate to the zero concentration of BRCT-Abraxas2p data using the ZeroConc module and to calculate R_g & $I(0)$ using the AutoRg module and pair-distribution functions & D_{max} using the AutoGNOM module (Figure S4C) (Petoukhov et al., 2012). Ten dummy-residue models of BRCT-Ab2p were created using DAMMIN (Svergun, 1999) and were superimposed and averaged using SUPCOMB (Kozin and Svergun, 2001) and DAMAVER (Volkov and Svergun, 2003) to generate a dummy-residue model of BRCT-Ab2p. The mean value of normalized-spatial discrepancy was 0.567. The selection of the best-fit model was conducted as follows. The missing N-termini of the BRCT domains and the peptide from BRCT-Ab2p crystal structure were added by *Coot* (Emsley et al., 2010). RapperTK (Gore et al., 2007) was used to generated 100 conformations of these flexible structures. A conformation of each chain was randomly selected and mixed to generate 1000 conformations of BRCT-Ab2p. The fitting of each conformation was calculated using CRYSOL to select the best conformation.

Supplemental References

Campbell, S.J., Edwards, R.A., and Glover, J.N.M. (2010). Comparison of the structures and peptide binding specificities of the BRCT domains of MDC1 and BRCA1. Structure *18*, 167–176.

Clapperton, J.A., Manke, I.A., Lowery, D.M., Ho, T., Haire, L.F., Yaffe, M.B., and Smerdon, S.J. (2004). Structure and mechanism of BRCA1 BRCT domain recognition of phosphorylated BACH1 with implications for cancer. Nat. Struct. Mol. Biol. *11*, 512–518.

Emsley, P., Lohkamp, B., Scott, W.G., and Cowtan, K. (2010). Features and development of Coot. Acta Crystallogr. D. Biol. Crystallogr. *66*, 486–501.

Fu, Y., Sander, J.D., Reyon, D., Cascio, V.M., and Joung, J.K. (2014). Improving CRISPR-Cas nuclease specificity using truncated guide RNAs. Nat Biotech *32*, 279–284.

Gore, S.P., Karmali, A.M., and Blundell, T.L. (2007). Rappertk: a versatile engine for discrete restraint-based conformational sampling of macromolecules. BMC Struct. Biol. *7*.

Kozin, M.B., and Svergun, D.I. (2001). Automated matching of high- and low-resolution structural models. J. Appl. Crystallogr. *34*, 33–41.

Krissinel, E., and Henrick, K. (2007). Inference of macromolecular assemblies from crystalline state. J. Mol. Biol. *372*, 774–797.

Liu, X., and Ladias, J.A.A. (2013). Structural basis for the BRCA1 BRCT interaction with the proteins ATRIP and BAAT1. Biochemistry *52*, 7618–7627.

Nakasako, M., Iwata, T., Inoue, K., and Tokutomi, S. (2005). Light-induced global structural changes in phytochrome A regulating photomorphogenesis in plants. FEBS J. *272*, 603–612.

Peränen, J., Rikkonen, M., Hyvönen, M., and Kääriäinen, L. (1996). T7 vectors with modified T7lac promoter for expression of proteins in Escherichia coli. Anal. Biochem. *236*, 371–373.

Petoukhov, M. V., Franke, D., Shkumatov, A. V., Tria, G., Kikhney, A.G., Gajda, M., Gorba, C., Mertens, H.D.T., Konarev, P. V., and Svergun, D.I. (2012). New developments in the ATSAS program package for small-angle scattering data analysis. J. Appl. Crystallogr. *45*, 342–350.

Ran, F.A., Hsu, P.D., Wright, J., Agarwala, V., Scott, D.A., and Zhang, F. (2013). Genome engineering using the CRISPR-Cas9 system. Nat. Protoc. *8*, 2281–2308.

Shen, Y., and Tong, L. (2008). Structural evidence for direct interactions between the BRCT domains of human BRCA1 and a phospho-peptide from human ACC1. Biochemistry *47*, 5767–5773.

Shiozaki, E.N., Gu, L., Yan, N., and Shi, Y. (2004). Structure of the BRCT repeats of BRCA1 bound to a BACH1 phosphopeptide: implications for signaling. Mol. Cell *14*, 405–412.

Svergun, D.I. (1999). Restoring Low Resolution Structure of Biological Macromolecules from Solution Scattering Using Simulated Annealing. *76*, 2879–2886.

Varma, A.K., Brown, R.S., Birrane, G., and Ladias, J.A.A. (2005). Structural Basis for Cell Cycle Checkpoint Control by the BRCA1−CtIP Complex. Biochemistry *44*, 10941–10946.

Volkov, V. V, and Svergun, D.I. (2003). Uniqueness of ab initio shape determination in small-angle scattering. J. Appl. Crystallogr. *36*, 860–864.

Wang, B., Matsuoka, S., Ballif, B.A., Zhang, D., Smogorzewska, A., Gygi, S.P., and Elledge, S.J. (2007). Abraxas and RAP80 Form a BRCA1 Protein Complex Required for the DNA Damage Response. Science (80-.). *316*, 1194–1198.

Williams, R.S., Lee, M.S., Hau, D.D., and Glover, J.N.M. (2004). Structural basis of phosphopeptide recognition by the BRCT domain of BRCA1. Nat Struct Mol Biol *11*, 519–525.